

References

1. Omori S, Tanaka Y, Takahashi A, Hirose H, Kashiwagi A, Kaku K, Kawamori R, Nakamura Y, Maeda S (2008) Association of CDKAL1, IGF2BP2, CDKN2A/B, HHEX, SLC30A8, and KCNJ11 with susceptibility to type 2 diabetes in a Japanese population. *Diabetes* 57: 791-795.
2. Stumvoll M, Goldstein BJ, van Haeften TW (2008) Type 2 diabetes: pathogenesis and treatment. *Lancet* 371: 2153-2156.
3. Bonnefond A, Froguel P, Vaxillaire M (2010) The emerging genetics of type 2 diabetes. *Trends Mol Med* 16: 407-416.
4. McCarthy MI, Zeggini E (2009) Genome-wide association studies in type 2 diabetes. *Curr Diab Rep* 9: 164-171.
5. Billings LK, Florez JC (2010) The genetics of type 2 diabetes: what have we learned from GWAS? *Ann N Y Acad Sci* 1212: 59-77.
6. Diabetes Genetics Initiative of Broad Institute of Harvard and MIT, Lund University, Novartis Institutes of BioMedical Research (2007) Genome-wide association analysis identifies loci for type 2 diabetes and triglyceride levels. *Science* 316: 1331-1336.
7. Steinthorsdottir V *et al* (2007) A variant in CDKAL1 influences insulin response and risk of type 2 diabetes. *Nat Genet* 39: 770-775.
8. Sim X, Ong RT, Suo C, Tay WT, Liu J, Ng DP, Boehnke M, Chia KS, Wong TY, Seielstad M, Teo YY, Tai ES (2011) Transferability of type 2 diabetes implicated loci in multi-ethnic cohorts from Southeast Asia. *PLoS Genet* 7: e1001363.
9. Stancáková A, Pihlajamäki J, Kuusisto J, Stefan N, Fritsche A, Häring H, Andreozzi F, Succurro E, Sesti G, Boesgaard TW, Hansen T, Pedersen O, Jansson PA, Hammarstedt A, Smith U, Laakso M; EUGENE2 Consortium (2008) Single-nucleotide polymorphism rs7754840 of CDKAL1 is associated with impaired insulin secretion in nondiabetic offspring of type 2 diabetic subjects and in a large sample of men with normal glucose tolerance. *J Clin Endocrinol Metab* 93: 1924-1930.
10. Zeggini E, Weedon MN, Lindgren CM, Frayling TM, Elliott KS, Lango H, Timpson NJ, Perry JR, Rayner NW, Freathy RM, Barrett JC, Shields B, Morris AP, Ellard S, Groves CJ, Harries LW, Marchini JL, Owen KR, Knight B, Cardon LR, Walker M, Hitman GA, Morris AD, Doney AS; Wellcome Trust Case Control Consortium (WTCCC), McCarthy MI, Hattersley AT (2007) Replication of genome-wide association signals in UK samples reveals risk loci for type 2 diabetes. *Science* 316: 1336-1341.
11. Miyaki K, Oo T, Song Y, Lwin H, Tomita Y, Hoshino H, Suzuki N, Muramatsu M (2010) Association of a cyclin-dependent kinase 5 regulatory subunit-associated protein 1-like 1 (CDKAL1) polymorphism with elevated hemoglobin A_{1c} levels and the prevalence of metabolic syndrome in Japanese men: interaction with dietary energy intake. *Am J Epidemiol* 172: 985-991.
12. Groenewoud MJ, Dekker JM, Fritsche A, Reiling E, Nijpels G, Heine RJ, Maassen JA, Machicao F, Schäfer SA, Häring HU, 't Hart LM, van Haeften TW (2008) Variants of CDKAL1 and IGF2BP2 affect first-phase insulin secretion during hyperglycaemic clamps. *Diabetologia* 51: 1659-1663.
13. Takeuchi F, Serizawa M, Yamamoto K, Fujisawa T, Nakashima E, Ohnaka K, Ikegami H, Sugiyama T, Katsuya T, Miyagishi M, Nakashima N, Nawata H, Nakamura J, Kono S, Takayanagi R, Kato N (2009) Confirmation of multiple risk loci and genetic impacts by a genome-wide association study of type 2 diabetes in the Japanese population. *Diabetes* 58: 1690-1699.
14. Fukushima M, Suzuki H, Seino Y (2004) Insulin secretion capacity in the development from normal glucose tolerance to type 2 diabetes. *Diabetes Res Clin Pract* 66: S37-43.
15. Fukushima M, Usami M, Ikeda M, Nakai Y, Taniguchi A, Matsuura T, Suzuki H, Kurose T, Yamada Y, Seino Y (2004) Insulin secretion and insulin sensitivity at different stages of glucose tolerance: a cross-sectional study of Japanese type 2 diabetes. *Metabolism* 53: 831-835.
16. Ching YP, Pang AS, Lam WH, Qi RZ, Wang JH (2002) Identification of a neuronal Cdk5 activator-binding protein as Cdk5 inhibitor. *J Biol Chem* 277: 15237-15240.
17. Wei FY, Nagashima K, Ohshima T, Saheki Y, Lu YF, Matsushita M, Yamada Y, Mikoshiba K, Seino Y, Matsui H, Tomizawa K (2005) Cdk5-dependent regulation of glucose-stimulated insulin secretion. *Nat Med* 11: 1104-1108.
18. Ubeda M, Rukstalis JM, Habener JF (2006) Inhibition of cyclin-dependent kinase 5 activity protects pancreatic beta cells from glucotoxicity. *J Biol Chem* 281: 28858-28864.
19. Ohara-Imaizumi M, Yoshida M, Aoyagi K, Saito T, Okamura T, Takenaka H, Akimoto Y, Nakamichi Y, Takanashi-Yanobu R, Nishiwaki C, Kawakami H, Kato N, Hisanaga S, Kakei M, Nagamatsu S (2010) Deletion of CDKAL1 affects mitochondrial ATP generation and first-phase insulin exocytosis. *PLoS One* 5: e15553.
20. Wei FY, Suzuki T, Watanabe S, Kimura S, Kaitsuka T, Fujimura A, Matsui H, Atta M, Michiue H, Fontecave M, Yamagata K, Suzuki T, Tomizawa K (2011) Deficit of tRNA^{Lys} modification by Cdkal1 causes the development of type 2 diabetes in mice. *J Clin Invest* 121: 3598-3608.
21. Arragain S, Handelman SK, Forouhar F, Wei FY, Tomizawa K, Hunt JF, Douki T, Fontecave M, Mulliez E,

- Atta M (2010) Identification of eukaryotic and prokaryotic methylthiotransferase for biosynthesis of 2-methylthio-N6-threonylcarbamoyladenine in tRNA. *J Biol Chem* 285: 28425-28433.
22. Pierrel F, Douki T, Fontecave M, Atta M (2004) MiaB protein is a bifunctional radical-S-adenosylmethionine enzyme involved in thiolation and methylation of tRNA. *J Biol Chem* 279: 47555-47663.
 23. Anton BP, Saleh L, Benner JS, Raleigh EA, Kasif S, Roberts RJ (2008) RimO, a MiaB-like enzyme, methylthiolates the universally conserved Asp88 residue of ribosomal protein S12 in *Escherichia coli*. *Proc Natl Acad Sci USA* 105: 1826-1831.
 24. Lee KH, Saleh L, Anton BP, Madinger CL, Benner JS, Iwig DF, Roberts RJ, Krebs C, Booker SJ (2009) Characterization of RimO, a new member of the methylthiotransferase subclass of the radical SAM superfamily. *Biochemistry* 48: 10162-10174.
 25. Arragain S, Garcia-Serres R, Blondin G, Douki T, Clemancey M, Latour JM, Forouhar F, Neely H, Montelione GT, Hunt JF, Mulliez E, Fontecave M, Atta M (2010) Post-translational modification of ribosomal proteins: structural and functional characterization of RimO from *Thermotoga maritima*, a radical S-adenosylmethionine methylthiotransferase. *J Biol Chem* 285: 5792-5801.
 26. Sofia HJ, Chen G, Hetzler BG, Reyes-Spindola JF, Miller NE (2001) Radical SAM, a novel protein superfamily linking unresolved steps in familiar biosynthetic pathways with radical mechanisms: functional characterization using new analysis and information visualization methods. *Nucleic Acids Res* 29: 1097-1106.
 27. Atta M, Mulliez E, Arragain S, Forouhar F, Hunt JF, Fontecave M (2010) S-Adenosylmethionine-dependent radical-based modification of biological macromolecules. *Curr Opin Struct Biol* 20: 684-692.
 28. Anantharaman V, Koonin EV, Aravind L (2001) TRAM, a predicted RNA-binding domain, common to tRNA uracil methylation and adenine thiolation enzymes. *FEMS Microbiol Lett* 197: 215-221.
 29. Hernández HL, Pierrel F, Elleingand E, García-Serres R, Huynh BH, Johnson MK, Fontecave M, Atta M (2007) MiaB, a bifunctional radical-S-adenosylmethionine enzyme involved in the thiolation and methylation of tRNA, contains two essential [4Fe-4S] clusters. *Biochemistry* 46: 5140-5147.
 30. Urbonavicius J, Qian Q, Durand JM, Hagervall TG, Björk GR (2001) Improvement of reading frame maintenance is a common function for several tRNA modifications. *EMBO J* 20: 4863-4873.
 31. Wilson RK, Roe BA (1989) Presence of the hypermodified nucleotide N6-(delta2-isopentenyl)-2-methylthioadenosine prevents codon misreading by *Escherichiacoli* phenylalanyl-transfer RNA. *Proc. Natl. Acad. Sci. U. S. A.* 86:409-413.
 32. Jenner LB, Demeshkina N, Yusupova G, Yusupov M (2010) Structural aspects of messenger RNA reading frame maintenance by the ribosome. *Nat Struct Mol Biol* 17: 555-560.
 33. McCrate NE, Varner ME, Kim KI, Nagan MC (2006) Molecular dynamics simulations of human tRNA^{Lys,3}UUU: the role of modified bases in mRNA recognition. *Nucleic Acids Res* 34: 5361-5368.
 34. Laybutt DR, Preston AM, Akerfeldt MC, Kench JG, Busch AK, Biankin AV, Biden TJ (2007) Endoplasmic reticulum stress contributes to β cell apoptosis in type 2 diabetes. *Diabetologia* 50: 752-763.
 35. Wang J, Takeuchi T, Tanaka S, Kubo SK, Kayo T, Lu D, Takata K, Koizumi A, Izumi T (1999) A mutation in the insulin 2 gene induces diabetes with severe pancreatic beta-cell dysfunction in the Mody mouse. *J. Clin. Invest.* 103:27-37.
 36. Yoshioka M, Kayo T, Ikeda T, Koizumi A (1997) A novel locus, Mody4, distal to D7Mit189 on chromosome 7 determines early-onset NIDDM in nonobese C57BL/6 (Akita) mutant mice. *Diabetes*. 46:887-894.
 37. Marchetti P, Bugliani M, Lupi R, Marselli L, Masini M, Boggi U, Filipponi F, Weir GC, Eizirik DL, Cnop M (2007) The endoplasmic reticulum in pancreatic b-cells of type2 diabetes patients. *Diabetologia* 50: 2486-2494.
 38. Kirchoff K, Machicao F, Haupt A, Schäfer SA, Tschritter O, Staiger H, Stefan N, Häring HU, Fritsche A (2008) Polymorphisms in the TCF7L2, CDKAL1 and SLC30A8 genes are associated with impaired proinsulin conversion. *Diabetologia*. 51:597-601.
 39. Stancáková A, Kuulasmaa T, Paananen J, Jackson AU, Bonnycastle LL, Collins FS, Boehnke M, Kuusisto J, Laakso M. (2009) Association of 18 confirmed susceptibility loci for type 2 diabetes with indices of insulin release, proinsulin conversion, and insulin sensitivity in 5,327 nondiabetic Finnish men. *Diabetes*. 58:2129-2136.

Development of type 2 diabetes caused by a deficiency of a tRNA^{lys} modification

Fan-Yan Wei and Kazuhito Tomizawa*

Department of Molecular Physiology; Faculty of Life Sciences; Kumamoto University; Kumamoto, Japan

Genetic variations in the *cdk5 regulator associated protein 1-like 1* (*cdkal1*) gene have been identified in whole genome association studies as a risk factor for the development of type 2 diabetes (T2D). A recent study showed that Cdkal1 was a mammalian methyltransferase, which specifically synthesizes 2-methylthio-N⁶-threonylcarbamoyladenosine (ms²t⁶A) at position 37 of tRNA^{lys}(UUU). The ms²t⁶A modification in tRNA^{lys}(UUU) was important for the accurate decoding of its cognate codon. In pancreatic β -cell-specific Cdkal1 knockout (Cdkal1 KO) mice, a deficiency of ms²t⁶A caused the mistranslation of a Lys codon in proinsulin, resulting in improper processing. The mice showed a decrease in insulin secretion and glucose intolerance. In addition, the mistranslation contributed to the expression of the endoplasmic reticulum (ER) stress response in Cdkal1-deficient β -cells. Furthermore, Cdkal1 KO mice were hypersensitive to high-fat diet-induced glucose intolerance, as well as the ER stress response. These findings might potentially explain the molecular pathogenesis of T2D in patients carrying *Cdkal1* variations.

Cdkal1 as a Risk Factor for T2D

Recent advances in whole-genome association studies (GWAS) have resulted in the identification of a number of genes associated with T2D. Among these risk genes, *cdkal1* is one of the most reproducible across different ethnic populations. To date, five single nucleotide polymorphisms (SNPs) in intron 5 of

cdkal1 (rs4712523, rs10946398, rs7754840, rs7756992 and rs9465871) have been shown to significantly influence the risk of T2D.^{1–4} Subsequent follow-up studies have found that the SNPs in *cdkal1* are associated with decreased insulin secretion, but not peripheral insulin sensitivity.^{5,6} For example, homozygous carriers of the risk allele rs7756992 have 22% lower insulin secretion than non-risk allele carriers.¹ Among nondiabetic offspring of T2D patients, carriers of GG and CC genotypes of rs7754840 had 11 and 24% lower first-phase insulin release than carriers of the GG genotype.⁷ At present, the biological function of the intronic SNPs in *cdkal1* is largely unknown. Recent studies have found that SNPs in *transcription factor 7-like 2* (*tcf7l2*), another T2D risk gene, were associated with a distinct alternative splicing pattern of *tcf7l2* mRNA.⁸ Thus, it is conceivable that the SNPs in *cdkal1* also regulate the expression pattern of *cdkal1* mRNA, which would ultimately affect insulin secretion in pancreatic β -cells.

Methylthiolation of tRNA^{lys}(UUU) by Cdkal1

Cdkal1 shares considerable domain and amino acid homology with Cdk5 regulator subunit-associated protein (Cdk5Rap1).⁹ Because Cdk5 is implicated in insulin secretion in pancreatic β -cells,¹⁰ Cdkal1 may regulate insulin secretion through interaction with Cdk5. However, unlike Cdk5Rap1, Cdkal1 is not involved in Cdk5-dependent signaling.¹¹

Cdkal1 contains several typical domains conserved in the methylthiotransferase (MTTase) family; the UPF0004, radical

Keywords: Cdkal1, islet, tRNA, translation, ER stress

Submitted: 9/23/11

Revised: 9/27/11

Accepted: 9/29/11

<http://dx.doi.org/10.4161/isl.4.1.18262>

*Correspondence to: Kazuhito Tomizawa;
Email: tomikt@kumamoto-u.ac.jp

Addendum to: Wei FY, Suzuki T, Watanabe S, Kimura S, Kaitsuka T, Fujimura A, et al. Deficit of tRNA^{lys} modification by Cdkal1 causes the development of type 2 diabetes in mice. *J Clin Invest* 2011; 121:3598–608; PMID:21841312; <http://dx.doi.org/10.1172/JCI58056>

S-adenosyl-L-methionine (SAM) and TRAM domain. Enzymes in the MTTase family catalyze chemically challenging reactions, involving a C-H to C-SCH₃ conversion.⁹ The UPF0004 domain and SAM domain utilize [4Fe-4S] clusters to generate the highly reactive 5'-deoxyadenosyl radical, which is necessary for C-SCH₃ to form. In addition to the conserved domains, Cdkal1 contains a unique hydrophobic domain at the C-terminus, which allows the protein to localize to the endoplasmic reticulum (ER) membrane.¹¹

Methylthiolation (ms²) by the MTTase family has been observed in tRNA and ribosomal protein.^{12,13} For example, MiaB, a bacterial protein, catalyzes the methylthiolation of N⁶-isopentenyladenosine (i⁶A) to generate 2-methyl-thio-N⁶-isopentenyladenosine (ms²i⁶A) at position 37 (A³⁷), 3'-adjacent to the anticodon in some tRNAs.¹² In amino acid sequence, MiaB shares high homology with the bacterial protein YqeV and its mammalian homolog Cdkal1. Both YqeV and Cdkal1 specifically catalyze the methylthiolation of N⁶-threonyl-carbamoyladenosine (t⁶A) to synthesize 2-methylthio-N⁶-threonyl-carbamoyladenosine (ms²t⁶A) at A³⁷ in tRNA^{Lys}(UUU).⁹

The Physiological Role of Methylthiolation in tRNA

The methylthiolation of A³⁷ in tRNA is critical for regulating decoding fidelity. For example, the ms²i⁶A modification is important for preventing the misreading and frame-shifting of cognate codons during translation in bacteria.^{14,15} Crystal structural analysis has revealed that the methylthiolation of i⁶A stabilizes the codon-anticodon interaction through cross-strand stacking with the base of the first nucleotide of the mRNA codon, which thus prevents mistranslation.¹⁶

Because the chemical structure of ms²t⁶A is highly similar to that of ms²i⁶A,^{16,17} it is conceivable that the ms² modification of t⁶A in tRNA^{Lys}(UUU) is also critical for preventing mistranslation of the Lys codon. By using a luciferase-based assay system, we have shown the ms² modification in tRNA^{Lys}(UUU) to be critical for preventing misreading of Lys.¹¹

Firefly luciferase was utilized as a reporter for examining the decoding fidelity of the Lys codon, because previous studies have shown that tLys529 in firefly luciferase is essential for its activity. In *yqeV*-deficient cells of *Bacillus subtilis* ($\Delta yqeV$), which lack the ms² modification in tRNA^{Lys}(UUU), we observed a significant decrease in firefly luciferase activity.¹¹ Notably, enhancement of the translation rate resulted in a further decrease in luciferase activity. These results suggest that the ms² modification in tRNA^{Lys}(UUU) is important for preventing misreading of the Lys codon, especially when the translation rate is high.

Pancreatic β -cell Dysfunction in Mice Lacking the ms² Modification of tRNA^{Lys}(UUU)

Precisely controlled proinsulin translation is critical for maintaining functional pancreatic β -cells. In *Akita* mice, mutation of the *proinsulin* gene directly causes a severe diabetic phenotype due to the presence of misfolded proinsulin.^{18,19} In transgenic mice in which Ser51 in eukaryotic initiation factor 2 α subunit (eIF2 α) was mutated to alanine, moreover, abnormally enhanced translation caused β -cell failure due to heightened and unregulated proinsulin translation.²⁰ Thus, abnormal translation of proinsulin subsequently evokes an ER stress response in β -cells, which ultimately disrupts the function of β -cells.

Human proinsulin, as well as mouse insulin I, contains two Lys residues. One of them is located in the cleavage site between the C-peptide and the A chain. We hypothesized that the mistranslation of the critical Lys codon in proinsulin might inhibit the cleavage and generate mis-folded proinsulin, which in turn might impair the function of β -cells. We generated Cdkal1 KO mice, in which the ms² modification in tRNA^{Lys}(UUU) was ablated in β -cells.¹¹ In the islets of Cdkal1 KO mice, a significant decrease in the incorporation of lysine into proinsulin as well as C-peptide production was observed. These observations suggest that a lack of the ms² modification in tRNA^{Lys}(UUU) in β -cells causes mistranslation of the Lys codon in proinsulin, resulting in the inhibition of subsequent processing. Furthermore, accumulation of mistranslated and misfolded proinsulin in Cdkal1 KO islets induced ER stress response as well as defective intracellular trafficking of secretory and plasma membrane proteins. Consequently, Cdkal1 KO mice exhibited glucose intolerance and a decrease in first-phase insulin secretion, which were also observed in Cdkal1 *null* mice. In addition, Cdkal1 KO mice fed a high-fat diet developed severe glucose intolerance due to a severe ER stress response in β -cells.

In summary, Cdkal1, a T2D risk factor, is a novel tRNA-modifying enzyme. The ms² modification of tRNA^{Lys}(UUU) by

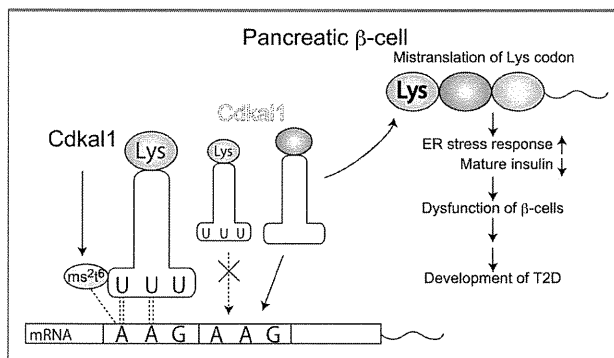


Figure 1. Schematic model of regulation of β -cell function by Cdkal1. Cdkal1 methylthiolates tRNA^{Lys}(UUU) at A³⁷, which stabilizes the interaction between tRNA^{Lys}(UUU) and its cognate codon AAG as well as AAA. Deficient of ms²t⁶A modification in tRNA^{Lys}(UUU) by Cdkal1 deficiency causes mistranslation of Lys codon in Proinsulin, which induce ER stress response and reduce mature insulin content in β -cells. Dysfunction of β -cells by Cdkal1 deficiency would ultimately lead to the development of T2D.

Cdkal1 is important for preventing mistranslation of the Lys codon. A deficiency of the ms^2 modification in Cdkal1 KO mice caused a mistranslation of Lys in the *proinsulin* gene, which in turn induced an ER stress response and affected the function of β -cells. Cdkal1 KO mice showed glucose intolerance and decreased

first-phase insulin secretion, which resemble the features of homozygous carriers of risk *cdkal1* SNPs (Fig. 1). Taken together, the mistranslation in β -cells caused by a deficiency of the ms^2 modification of tRNA^{Lys}(UUU) may underline the molecular pathogenesis of T2D in patients carrying risk *cdkal1*

SNPs. Consistent with this hypothesis, recent studies also found that proinsulin conversion was decreased in homozygous carriers of risk *cdkal1* SNPs.^{21,22} Further studies in human samples are needed to examine whether the risk *cdkal1* SNPs are associated with the level of ms^2 modification.

References

- Steinthorsdottir V, Thorleifsson G, Reynisdottir I, Benediktsson R, Jonsdottir T, Walters GB, et al. Variant in CDKAL1 influences insulin response and risk of type 2 diabetes. *Nat Genet* 2007; 39:770-5; PMID:17460697; <http://dx.doi.org/10.1038/ng2043>
- Diabetes Genetics Initiative of Broad Institute of Harvard and MIT, Lund University, and Novartis Institutes of BioMedical Research, Saxena R, Voight BF, Lyssenko V, et al. Genome-wide association analysis identifies loci for type 2 diabetes and triglyceride levels. *Science* 2007; 316:1331-6; PMID:17463246; <http://dx.doi.org/10.1126/science.1142358>
- Scott LJ, Mohlke KL, Bonnycastle LL, Willer CJ, Li Y, Duren WL, et al. A genome-wide association study of type 2 diabetes in Finns detects multiple susceptibility variants. *Science* 2007; 316:1341-5; PMID:17463248; <http://dx.doi.org/10.1126/science.1142382>
- Zeggini E, Weedon MN, Lindgren CM, Frayling TM, Elliott KS, Lango H, et al. Replication of genome-wide association signals in UK samples reveals risk loci for type 2 diabetes. *Science* 2007; 316:1336-41; PMID:17463249; <http://dx.doi.org/10.1126/science.1142364>
- Groenewoud MJ, Dekker JM, Fritsche A, Reiling E, Nijpels G, Heine RJ, et al. Variants of CDKAL1 and IGF2BP2 affect first-phase insulin secretion during hyperglycaemic clamps. *Diabetologia* 2008; 51:1659-63; PMID:18618095; <http://dx.doi.org/10.1007/s00125-008-1083-z>
- Ruchat SM, Elks CE, Loos RJ, Vohl MC, Weisnagel SJ, Rankinen T, et al. Association between insulin secretion, insulin sensitivity and type 2 diabetes susceptibility variants identified in genome-wide association studies. *Acta Diabetol* 2009; 46:217-26; PMID:19082521; <http://dx.doi.org/10.1007/s00592-008-0080-5>
- Stancáková A, Pihlajamäki J, Kuusisto J, Stefan N, Fritsche A, Häring H, et al. Single-nucleotide polymorphism rs7754840 of CDKAL1 is associated with impaired insulin secretion in nondiabetic offspring of type 2 diabetic subjects and in a large sample of men with normal glucose tolerance. *J Clin Endocrinol Metab* 2008; 93:1924-30; PMID:18285412; <http://dx.doi.org/10.1210/jc.2007-2218>
- Le Bacquer O, Shu L, Marchand M, Neve B, Paroni F, Kerr Conte J, et al. TCF7L2 splice variants have distinct effects on beta-cell turnover and function. *Hum Mol Genet* 2011; 20:1906-15; PMID:21357677; <http://dx.doi.org/10.1093/hmg/ddr072>
- Arragain S, Handelman SK, Forouhar F, Wei FY, Tomizawa K, Hunt JF, et al. Identification of eukaryotic and prokaryotic methyltransferase for biosynthesis of 2-methylthio-N6-threonylcarbamoyladenosine in tRNA. *J Biol Chem* 2010; 285:28425-33; PMID:20584901; <http://dx.doi.org/10.1074/jbc.M110.106831>
- Wei FY, Nagashima K, Ohshima T, Saheki Y, Lu YF, Matsushita M, et al. Cdk5-dependent regulation of glucose-stimulated insulin secretion. *Nat Med* 2005; 11:1104-8; PMID:16155576; <http://dx.doi.org/10.1038/nm1299>
- Wei FY, Suzuki T, Watanabe S, Kimura S, Kaitsuka T, Fujimura A, et al. Deficit of Lys-tRNA modification by Cdkal1 causes the development of type 2 diabetes in mice. *J Clin Invest* 2011; 121:3598-608; PMID:21841312; <http://dx.doi.org/10.1172/JCI58056>
- Pierrel F, Douki T, Fontecave M, Atta M. MiaB protein is a bifunctional radical-S-adenosylmethionine enzyme involved in thiolation and methylation of tRNA. *J Biol Chem* 2004; 279:47555-63; PMID:15339930; <http://dx.doi.org/10.1074/jbc.M408562200>
- Anton BP, Saleh L, Benner JS, Raleigh EA, Kasif S, Roberts RJ, et al. MiaB-like enzyme, methylthiolates the universally conserved Asp88 residue of ribosomal protein S12 in *Escherichia coli*. *Proc Natl Acad Sci USA* 2008; 105:1826-31; PMID:18252828; <http://dx.doi.org/10.1073/pnas.0708608105>
- Urbonavicius J, Qian Q, Durand JM, Hagervall TG, Björk GR. Improvement of reading frame maintenance is a common function for several tRNA modifications. *EMBO J* 2001; 20:4863-73; PMID:11532950; <http://dx.doi.org/10.1093/emboj/20.17.4863>
- Wilson RK, Roe BA. Presence of the hypermodified nucleotide N6-(delta2-isopentenyl)-2-methylthioadenosine prevents codon misreading by *Escherichiacoli* phenylalanyl-transfer RNA. *Proc Natl Acad Sci USA* 1989; 86:409-13; PMID:2643111; <http://dx.doi.org/10.1073/pnas.86.2.409>
- Jenner LB, Demeshkina N, Yusupova G, Yusupov M. Structural aspects of messenger RNA reading frame maintenance by the ribosome. *Nat Struct Mol Biol* 2010; 17:555-60; PMID:20400952; <http://dx.doi.org/10.1038/nsmb.1790>
- McCrane NE, Varner ME, Kim KI, Nagan MC. Molecular dynamics simulations of human tRNA^{Lys}UUU: the role of modified bases in mRNA recognition. *Nucleic Acids Res* 2006; 34:5361-8; PMID:17012271; <http://dx.doi.org/10.1093/nar/gkl580>
- Wang J, Takeuchi T, Tanaka S, Kubo SK, Kayo T, Lu D, et al. mutation in the insulin 2 gene induces diabetes with severe pancreatic beta-cell dysfunction in the Mody mouse. *J Clin Invest* 1999; 103:27-37; PMID:9884331; <http://dx.doi.org/10.1172/JCI4431>
- Yoshioka M, Kayo T, Ikeda T, Koizumi A. A novel locus, Mody4, distal to D7Mit189 on chromosome 7 determines early-onset NIDDM in nonobese C57BL/6 (Akita) mutant mice. *Diabetes* 1997; 46:887-94; PMID:9133560; <http://dx.doi.org/10.2337/diabetes.46.5.887>
- Back SH, Scheuner D, Han J, Song B, Ribick M, Wang J, et al. Translation attenuation through eIF2alpha phosphorylation prevents oxidative stress and maintains the differentiated state in beta cells. *Cell Metab* 2009; 10:13-26; PMID:19583950; <http://dx.doi.org/10.1016/j.cmet.2009.06.002>
- Kirchhoff K, Machicao F, Haupt A, Schäfer SA, Tschritter O, Staiger H, et al. Polymorphisms in the TCF7L2, CDKAL1 and SLC30A8 genes are associated with impaired proinsulin conversion. *Diabetologia* 2008; 51:597-601; PMID:18264689; <http://dx.doi.org/10.1007/s00125-008-0926-y>
- Stancáková A, Kuulasmaa T, Paananen J, Jackson AU, Bonnycastle LL, Collins FS, et al. Association of 18 confirmed susceptibility loci for type 2 diabetes with indices of insulin release, proinsulin conversion, and insulin sensitivity in 5,327 nondiabetic Finnish men. *Diabetes* 2009; 58:2129-2136; PMID:19502414; <http://dx.doi.org/10.2337/db09-0117>

Novel Animal Glioma Models that Separately Exhibit Two Different Invasive and Angiogenic Phenotypes of Human Glioblastomas

Satoshi Inoue¹, Tomotsugu Ichikawa¹, Kazuhiko Kurozumi¹, Tomoko Maruo¹, Manabu Onishi¹, Koichi Yoshida¹, Kentaro Fujii¹, Hirokazu Kambara¹, E. Antonio Chiocca², Isao Date¹

Key words

- Angiogenesis
- Animal brain tumor model
- Glioma
- Invasion

Abbreviations and Acronyms

BBB: Blood-brain barrier
 cDNA: Complementary DNA
 CNS: Central nervous system
 DAB: Diaminobenzidine
 DAPI: 4',6-diamino-2-phenylindole
 DMEM: Dulbecco's modified Eagle's medium
 FBS: Fetal bovine serum
 GAPDH: Glycerolaldehyde 3-phosphate dehydrogenase
 GFP: Green fluorescent protein
 HIF-1: Hypoxia-inducible factor-1
 MAP: Microtubule-associated protein
 MMP-2: Matrix metalloproteinase-2
 MMP-9: Matrix metalloproteinase-9
 MRI: Magnetic resonance imaging
 PBS: Phosphate-buffered saline
 PCR: Polymerase chain reaction
 PDGF: Platelet-derived growth factor
 RECA-1: Rat endothelial cell antigen-1
 SPARC: Secreted protein acidic and rich in cysteine
 VEGF: Vascular endothelial growth factor



From the ¹Department of Neurological Surgery, Okayama University Graduate School of Medicine, Dentistry and Pharmaceutical Sciences, Okayama, Japan; and ²Dardinger Laboratory for Neuro-oncology and Neurosciences, Department of Neurological Surgery, James Comprehensive Cancer Center and The Ohio State University Medical Center, Columbus, Ohio, USA

To whom correspondence should be addressed:

Tomotsugu Ichikawa, M.D., Ph.D.
 [E-mail: tomoichi@cc.okayama-u.ac.jp]

Citation: *World Neurosurg.* (2012).

DOI: 10.1016/j.wneu.2011.09.005

Journal homepage: www.WORLDNEUROSURGERY.org

Available online: www.sciencedirect.com

1878-8750/\$ - see front matter © 2012 Elsevier Inc.
 All rights reserved.

INTRODUCTION

Malignant glioma is the most common primary brain tumor in adults. It is characterized by rapid expansion, invasion of adjacent central nervous system (CNS) tissues, and aberrant vascularization (32, 49). De-

OBJECTIVE: Invasive behaviors of malignant gliomas are fundamental traits and major reasons for treatment failure. Delineation of invasive growth is important in establishing treatment for gliomas and experimental neuro-oncology could benefit from an invasive glioma model. In this study, we established two new cell line-based animal models of invasive glioma.

METHODS: Two cell lines, J3T-1 and J3T-2, were derived from the same parental canine glioma cell line, J3T. These cells were inoculated to establish brain tumors in athymic mice and rats. Pathologic samples of these animal gliomas were examined to analyze invasive patterns in relation to angiogenesis, and were compared with human glioblastoma samples. The molecular profiles of these cell lines were also shown.

RESULTS: Histologically, J3T-1 and J3T-2 tumors exhibited different invasive patterns. J3T-1 cells clustered around newly developed vessels at tumor borders, whereas J3T-2 cells showed diffuse single cell infiltration into surrounding healthy parenchyma. In human malignant glioma samples, both types of invasion were observed concomitantly. Molecular profiles of these cell lines were analyzed by immunocytochemistry and with quantitative reverse transcription polymerase chain reaction. Vascular endothelial growth factor, matrix metalloproteinase-9, hypoxia-inducible factor-1, and platelet-derived growth factor were overexpressed in J3T-1 cells rather than in J3T-2 cells, whereas integrin $\alpha v \beta 3$, matrix metalloproteinase-2, nestin, and secreted protein acidic and rich in cysteine were overexpressed in J3T-2 cells rather than in J3T-1 cells.

CONCLUSIONS: These animal models histologically recapitulated two invasive and angiogenic phenotypes, namely angiogenesis-dependent and angiogenesis-independent invasion, also observed in human glioblastoma. These cell lines provided a reproducible in vitro and in vivo system to analyze the mechanisms of invasion and angiogenesis in glioma progression.

spite recent advances in treatment with surgery, radiation, and chemotherapy, patients with glioblastoma have less than 2-year median survival after diagnosis, and only 16.0% survive beyond 3 years (43).

Invasion by tumor cells into surrounding brain tissue is a major problem in managing malignant glioma. It is the reason why resection is not curative, it leads to relapse and death, and it has been investigated extensively (18). Almost 70 years ago, in a series of 120 untreated gliomas, Scherer (41) showed an infiltrative growth pattern that was associated with distinct anatomic

structures—tumor cells followed myelinated axons and the basement membranes of blood vessels (18).

Several factors make it difficult to analyze invasion. One is the lack of glioma-specific staining for pathologic analysis. Exact localization of invading glioma cells in seemingly healthy brain parenchyma is crucial for the precise evaluation of invasion patterns. Recently, microtubule-associated protein 2e (MAP2e), a splice variant of MAP-2, has been reported as a candidate glioma-specific antigen. Most cells in CNS tumors, particularly oligodendrogliomas

and glioblastomas, are intensely stained and permit visualization of invasive glioma cells (44). Another reason for difficulty in analyzing invasion is that there are few, if any, transplantable animal models that show an invasive growth pattern. Typically, transplantable tumors in mice or rats form solid nodules at the injection site, which compress rather than invade the surrounding brain (49).

Delineation of invasive growth is very important in establishing treatment for gliomas and experimental neuro-oncology could benefit from invasive glioma models that exhibit different histologic patterns (1, 8, 20).

In the present study, we established two new cell line-based animal models of invasive glioma that reflect the invasive phenotype of malignant gliomas in humans. Pathologic samples of these animal gliomas were examined to analyze invasive patterns in relation to angiogenesis and were compared with human glioblastoma samples. The molecular profiles of these animal models were also shown.

MATERIALS AND METHODS

Cell Preparation

J3T canine glioma cells were generous gift from Dr. Michael E. Berens (Translation Genomics Research Institute, Phoenix, Arizona, USA) (5). Two cell lines (J3T-1 and J3T-2) were developed from a parental J3T cell line, as previously described (22). Briefly, J3T cells (5×10^6) were implanted subcutaneously into the flanks of two athymic mice (NCR/Sed, nu/nu; 20 g). After 6 weeks, two tumors were established in two animals. Tumors were harvested in a sterile fashion, minced with a scalpel in 1-mm³ cubes, treated for 1 hour with 1 mg/mL collagenase/dispase (Roche, Basel, Switzerland) and subsequently cultured in Dulbecco's modified Eagle's medium (DMEM) supplemented with 10% fetal bovine serum (FBS), 100 units of penicillin, and 0.1 mg/mL of streptomycin. J3T-1 and J3T-2 cell lines were each derived from single subcutaneous tumors.

For enhanced visualization of J3T-1 and J3T-2 cells, we established cell lines that stably expressed green fluorescent protein (GFP). J3T-1 and J3T-2 cells were transfected with the pAcGFP1-C1 plasmid (Clontech Laboratories Inc., Mountain View, Cal-

ifornia, USA), which encoded GFP using TransIT-LTI reagent (Takara Bio Inc., Otsu, Shiga, Japan) to make J3T-1G and J3T-2G. Cells were cultured in DMEM supplemented with 10% FBS, 100 units of penicillin, and 0.1 mg/mL of streptomycin.

Animal Glioma Xenograft Model

All experimental animals were housed and handled in accordance with the Okayama University Animal Research Committee guidelines. Before implantation, 85% to 90% of confluent J3T-1, J3T-2, J3T-1G, and J3T-2G cells were trypsinized, rinsed with DMEM + 10% FBS, and centrifuged at 800 rpm for 5 minutes. The resulting pellet was resuspended in phosphate-buffered saline (PBS) and concentration was adjusted to 1×10^5 cells/ μ L of PBS. Athymic rats (F344/N-nu/nu CLEA Japan, Inc., Tokyo, Japan) and mice (balb/c-nu/nu; CLEA Japan, Inc.) were used for the animal experiments. To establish brain tumor models, animals were anesthetized with intraperitoneal nembutal (30 mg/kg) and placed in a stereotactic apparatus (Narishige, Tokyo, Japan). Tumor cells (athymic rat: 5×10^5 cells/ 5μ L, athymic mouse: 2×10^5 cells/ 2μ L) were slowly injected into the basal ganglia of the right cerebral hemisphere (athymic rat: 4 mm lateral and 1 mm anterior to the bregma at a depth of 4 mm; athymic mouse: 3 mm lateral and 1 mm anterior to the bregma at a depth of 3 mm) using a Hamilton syringe (Hamilton, Reno, Nevada, USA) according to previously published procedures (22, 27). For histologic examination, athymic rats (J3T-1: $n = 5$, J3T-2: $n = 5$) were sacrificed 4 to 5 weeks after tumor inoculation and fixed *in vivo* by transcardiac perfusion with 4% paraformaldehyde. Their brains were then removed and stored in 4% paraformaldehyde. To analyze survival time, we monitored xenograft models of J3T-1 ($n = 9$) and J3T-2 ($n = 8$) in athymic mice.

Immunofluorescence Analysis of Animal Brain Tumor Model

Animal brains were sliced into 16- μ m sections for pathologic examination. Fluorescence microscopy was used to visualize implanted glioma cells. Snap-frozen tissue samples were embedded in optimal cutting temperature compound for cryosectioning and sliced into 16- μ m sections for indirect

immunofluorescence. Slides were incubated with 10% horse serum in PBS at room temperature for 60 minutes and then incubated overnight at 4°C with anti-rat endothelial cell antigen-1 (RECA-1) antibody (1:20) (Abcam, Cambridge, Massachusetts, USA) diluted in PBS with 1% horse serum. After three washes with PBS, slides were incubated with anti-mouse IgG Cy3-conjugated antibody (Jackson ImmunoResearch Laboratories, Inc., West Grove, Pennsylvania, USA) and 4',6-diamino-2-phenylindole (DAPI; 1:500) (Invitrogen, Tokyo, Japan) in PBS for 60 minutes. After three washes, coverslips were mounted on the slides using Gel/Mount (Biomedica, Foster City, California, USA) and sections were examined using a fluorescence microscope equipped with triple fluorescent filter sets and a CCD camera connected to a computer.

Microvessel number and diameter were measured in 4-week-old brain tumors to assess angiogenic activity in these models (J3T-1, $n = 3$; J3T-2, $n = 3$). In both J3T-1 and J3T-2 xenograft models, five digital images were obtained ($\times 200$, 0.15 mm²) from areas at the tumor borders and in the contralateral normal basal ganglia. Image J software (<http://rsb.info.nih.gov/ij>) was used to measure the number and diameter of vessels in these images. Statistical significance of vessel number and diameter was examined using the Mann-Whitney U test. P value less than 0.05 was considered to be statistically significant. Statistical analysis was performed using StatView statistical software (version 5.0; SAS Institute Inc., Cary, North Carolina, USA).

Magnetic Resonance Imaging in Animal Models

Animal brain tumors were analyzed using T₁- and T₂-weighted magnetic resonance imaging (MRI) 5 weeks after tumor inoculation (J3T-1, $n = 4$; J3T-2, $n = 4$). Animals were anesthetized with nembutal (30 mg/kg) and placed in a quadrature transmit/receive head coil (diameter, 28 cm). Coronal T₁-weighted images (repetition time, 400 ms; echo time, 11 ms; 2-mm thickness/0.2-mm gap; field of view, 12 \times 12 cm; matrix, 256 \times 256; 2 excitations) and T₂-weighted images (repetition time, 3000 ms; echo time, 102 ms, 2-mm thickness/0.2-mm gap; field of view, 12 \times 12 cm; matrix 256 \times 256; 2 excitations) were obtained

with a 1.5-tesla superconducting magnet MRI device (Signa Advantage version 5.4, General Electric, Milwaukee, Wisconsin, USA). Furthermore, coronal T₁-weighted images were obtained after an intravenous injection of gadolinium-diethylenetriaminepenta acetic acid (1.0 mL/kg) using the same MRI device.

Immunocytochemistry of Cultured Cell

J3T-1 and J3T-2 tumor cells were plated onto coverslips and cultured for 24 hours. These cells were washed three times with PBS and fixed with 4% paraformaldehyde for 10 minutes. Nonspecific binding was blocked by 10% horse serum in PBS for 1 hour at room temperature. Subsequently, cells were incubated 90 minutes at room temperature with anti-vascular endothelial growth factor (VEGF) antibody (1:20) (R&D Systems, Minneapolis, Minnesota, USA) and anti-integrin αβ3 antibody (1:100) (Millipore, Billerica, Massachusetts, USA). Negative controls were treated similarly (time and temperature) with omission of the primary antibody. After washing, cells were incubated at room temperature with anti-mouse IgG Cy3-conjugated antibody (Jackson ImmunoResearch Laboratories, Inc., West Grove, Pennsylvania, USA) and DAPI (1:500) (Invitrogen) in PBS for 60 minutes. After three washes, coverslips were mounted on the slides using Gel/Mount (Biomed). Fluorescent microscope equipped with triple fluorescent filter sets and a CCD camera connected to a computer was used to visualize fluorescence and to take pictures.

Quantitative Reverse Transcription Polymerase Chain Reaction Analysis of Cultured Cell

Total RNA was isolated from cultured J3T-1 and J3T-2 cells using RNeasy Mini Kit (QIAGEN, Valencia, California, USA) and was reverse transcribed with oligo dT primers using SuperScript III First-Strand Synthesis System for reverse transcription-polymerase chain reaction (PCR; Invitrogen, Carlsbad, California, USA) according to manufacturer's instructions. Primers specific for each gene target were designed using Primer Express Software (Applied Biosystems, Foster City, California, USA) and synthesized by Invitrogen (Table 1). The result-

ing complementary DNA (cDNA) was amplified by PCR with gene-specific primers using 7300 Real Time PCR system (Applied Biosystems) and QuantiTect SYBR Green PCR Kit (QIAGEN). A log-linear relationship between amplification curve and quantity of cDNA in the range of 1 to 1000 copies were observed.

Quantification was done by Comparative Ct method using 7300 Real Time PCR System with Sequence Detection Software version 1.4 (Applied Biosystems). The cDNA amount in each sample was normalized to the crossing point of the housekeeping gene GAPDH (glyceraldehyde 3-phosphate dehydrogenase). Thermal cycling parameters were as follows: denaturation at 95 °C for 10 minutes followed by 40 cycles at 95 °C for 15 seconds and 60 °C for 1 minute. Relative messenger RNA fold up-regulation in J3T-2 cells for each gene was calculated using the respective crossing points applied in the following formula: $F = 2^{(A_H - A_G) - (B_H - B_G)}$ where F = fold difference, A = J3T-2 cells, B = J3T-1 cells, H = housekeeping (GAPDH), and G = gene of interest.

Histopathologic Examination of Human Surgical Specimens

From April 2004 to March 2005, five consecutive samples of human glioblastoma were surgically removed en bloc, including surrounding healthy brain parenchyma (Okayama University Hospital).

Glioma specimens were diagnosed and graded according to the World Health Organization classification of tumors of CNS by a neuropathologist. No patient received radiotherapy or chemotherapy before surgery.

Formalin-fixed and paraffin-embedded surgical specimens were sliced into 4-μm sections and mounted on microscopy slides (Thermo Fisher Scientific, Waltham, Massachusetts, USA) for histopathologic examination. After deparaffinization in xylene and rehydration in decreasing concentrations of ethanol, sections were incubated in 0.3% hydrogen peroxide (30 minutes) and treated with an autoclave for 10 minutes at 121°C in distilled water. After three washes in PBS, sections were incubated at room temperature with anti-MAP2e monoclonal antibody (1:20 mouse IgG₁; gift from Bridget Shafit-Zagardo, Albert Einstein College of Medicine, Bronx, New York, USA) diluted in a solution of PBS and 5% skim milk (60 minutes). After incubation, sections were rinsed with PBS and incubated with secondary antibody against mouse IgG, which was applied using the DakoCytomation Envision+ System-HRP kit according to manufacturer's protocol (DakoCytomation, Carpinteria, California, USA), and diaminobenzidine (DAB). After three washes in PBS, sections were incubated overnight at 4°C with anti-vWf polyclonal antibody (1:300 rabbit, A0082, DakoCytomation). After incubation, sections were rinsed with PBS and incubated with secondary antibody against rabbit IgG with the DakoCytomation Envision+ System-HRP kit. Deep purple staining was achieved with DAB-nickel (0.05 M Tris-buffered saline containing 0.03% DAB and 0.06% nickel ammonium sulfate). After three washes, coverslips were mounted on the slides, and sections were examined with a microscope equipped with a CCD camera connected to a computer.

Table 1. List of Primer Sequences

Primer Set	Forward	Reverse
GAPDH	CATCACTGCCACCCAGAAGA	AGTGGGTGCTACTGTTGAAGTCA
MMP-2	TGTAGTTAAATGGGCGTGCTCA	AAGTGCATACAAGCAAACCTGCTAA
MMP-9	CTCTGAGGCCCTACAGTGC	AAGCGGTCTGGCAGAAGTA
HIF-1	TTCTTGGAACGCGTAAAAGG	ACCAAGGAAGTGTGAAAATGTGCT
nestin	CACCCATAGAGCCTTCAACCC	ACCACATTCTCCCCCTCT
SPARC	GACGGGTACCTGTCCCACA	CCGTTAGTGGGTGAGCAAGAG
PDGF	GCCCGTTTACAGGTGAGAAAAA	GTGCTTGAAGTCCCGGTGCT

GAPDH, glyceraldehyde 3-phosphate dehydrogenase; HIF-1, hypoxia-inducible factor-1; MMP-2, matrix metalloproteinase-2; MMP-9, matrix metalloproteinase-9; PDGF, platelet-derived growth factor; SPARC, secreted protein acidic and rich in cysteine.

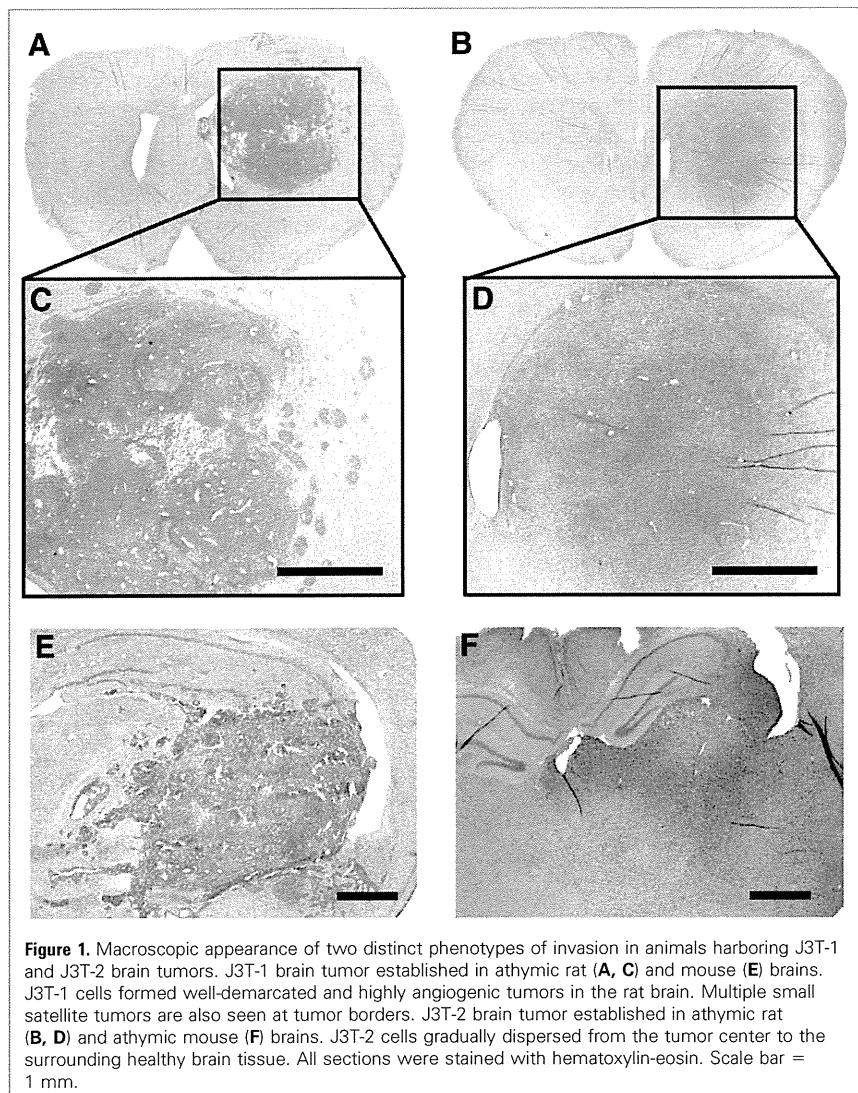


Figure 1. Macroscopic appearance of two distinct phenotypes of invasion in animals harboring J3T-1 and J3T-2 brain tumors. J3T-1 brain tumor established in athymic rat (A, C) and mouse (E) brains. J3T-1 cells formed well-demarcated and highly angiogenic tumors in the rat brain. Multiple small satellite tumors are also seen at tumor borders. J3T-2 brain tumor established in athymic rat (B, D) and athymic mouse (F) brains. J3T-2 cells gradually dispersed from the tumor center to the surrounding healthy brain tissue. All sections were stained with hematoxylin-eosin. Scale bar = 1 mm.

The degree of angiogenesis at the tumor borders, degree of perivascular MAP2e-positive cell cuffing, and density of single tumor cell infiltration in the cerebral cortex overlaying the tumor mass were determined. The degree of angiogenesis at the tumor borders was graded on a scale of 0 to 3+ as follows: 0, no detectable angiogenic activity; 1+, trace of dilated vessels; 2+, moderate number of dilated vessels; and 3+, high number of dilated vessels. Degree of perivascular MAP2e-positive cell cuffing was graded on a scale of 0 to 3+ as follows: 0, no detectable cuffing; 1+, patchy cuffing; 2+, near-circumferential thin cuffing; and 3+, circumferential thick cuffing. The density of single tumor cell infiltration in the cerebral cortex was graded on a scale of 0 to 3+ as follows: 0, no detectable tumor cells;

1+, sparse tumor cells at a density of less than 5 per high-power field; 2+, moderate tumor cells at a density of less than 20 per high-power field; and 3+, dense tumor cells at a density of >20 per high-power field. This classification was made by two neurosurgeons (S.I., T.M.) without prior knowledge of clinical or radiologic data of patients.

RESULTS

Two J3T Subclones Showed Different Invasive and Angiogenic Phenotypes in Animal Brains

Two subclones of the J3T canine glioma cell line, J3T-1 and J3T-2, were implanted in rat and mouse brains. Histologically, J3T-1 cells

and J3T-2 tumors exhibited different morphologies (Figure 1A–D). When tested in athymic mice, similar histologic patterns were observed (Figure 1E, F). J3T-1 cells formed well-demarcated and highly angiogenic tumors in rat brains. At the center of the tumor, regions of high angiogenic activity with large number of dilated vessels were present. Furthermore, necrotic foci and pseudopalisading tumor cells were also seen. In healthy parenchyma adjacent to the main tumor mass, multiple satellite tumor cells were seen with dilated blood vessels in them (Figure 2A). In contrast, J3T-2 cells formed poorly demarcated tumors. Tumor cells gradually dispersed from the tumor center to the healthy brain parenchyma with a gradient of cell density. Minimal angiogenesis was seen with a small number of slightly dilated vessels at the tumor center (Figure 2B). No dilated blood vessels or cluster of tumor cells were visible in areas distant from the tumor.

To facilitate tumor cell identification, J3T-1 and J3T-2 cells were transfected with the gene for GFP. In the J3T-1G model, cluster formation of tumor cells around dilated RECA-1-positive vessels was clearly shown by immunohistochemical staining (Figure 3A). No single cell infiltration was seen in the healthy brain. In the J3T-2G model, fluorescent microscopy clearly distinguished spindle-shaped tumor cells from normal glia or neuronal cells. Single cell infiltration independent of vasculature was seen in healthy brain tissue distant from the tumor center (Figure 3B, C). In the corpus callosum, stretched spindle cells turned in the direction of neuronal fibers and were distributed along them (Figure 3D). Spindle-shaped cells were also found dispersed along cortical axons.

Blood Vessel Morphology Differs Between J3T-1 and J3T-2 Tumors

To analyze the angiogenic activity in the invasive front of J3T-1 and J3T-2 brain tumors, brain sections were stained with RECA-1 and DAPI (Figure 4). In J3T-1 brain tumors, large and dilated vessels, which were recognized as neovascular vessels, were located at the tumor borders. On the contrary, in J3T-2 tumors, no dilated vessels were seen at the tumor borders. In J3T-1 and J3T-2 tumors, the number of vessels at the tumor borders did not increase compared with that in contralateral healthy brain tissue. In contrast, the diameter of vessels in

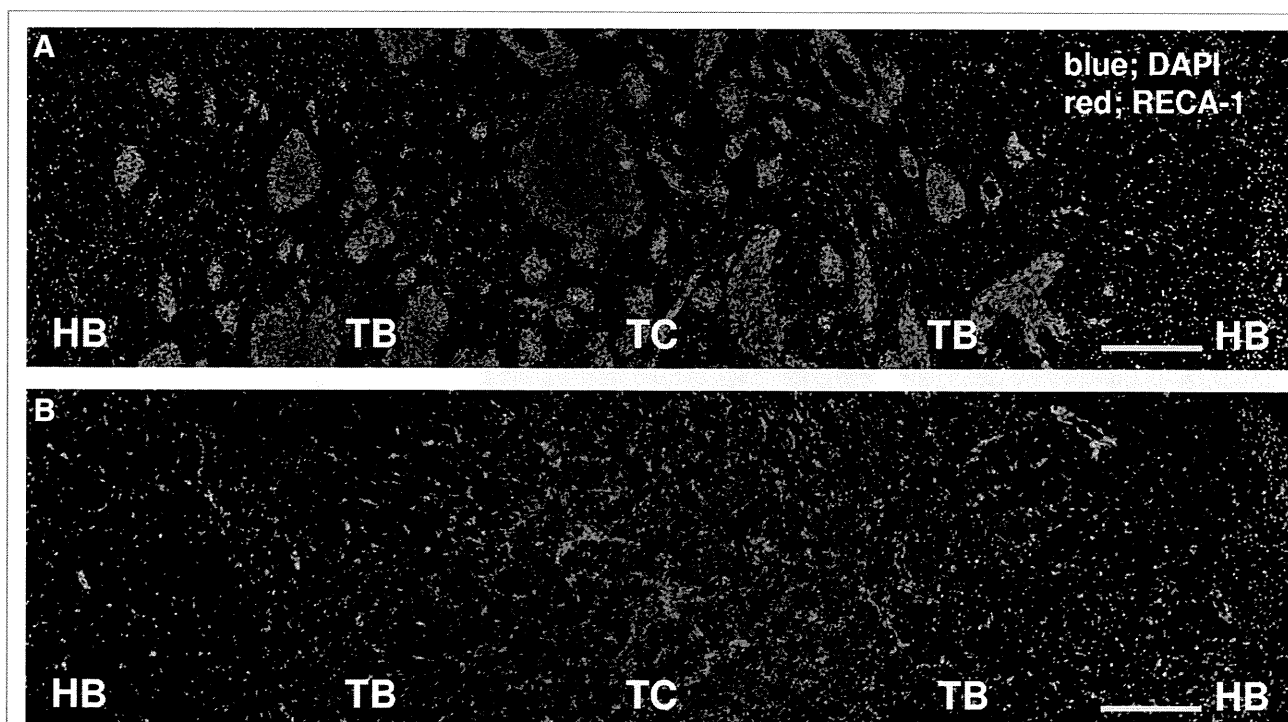


Figure 2. Fluorescent images of 4',6-diamino-2-phenylindole (DAPI) nuclear staining (blue) and RECA-1 immunohistochemical staining (red). **(A)** J3T-1 brain tumor. Dilated vessels are present in the satellite tumors at tumor

borders. **(B)** J3T-2 brain tumor. Dilated vessels at tumor borders are absent. Scale bar = 300 μ m. TC, tumor center; TB, tumor border; HB, healthy brain tissue.

J3T-1 tumors, but not in J3T-2 tumors, was significantly increased compared with that in contralateral healthy brain tissue (J3T-1 vs. J3T-2: 1.62 ± 0.36 -fold vs. 0.95 ± 0.14 -fold, respectively; $P < 0.05$).

MRI of Rats With J3T-1 and J3T-2

Tumors Showed Different Characteristics
MRI of rats with J3T-1 and J3T-2 tumors was performed 5 weeks after tumor inoculation. Gadolinium-diethylenetriaminepenta acetic acid-enhanced T_1 -weighted images of rats with J3T-1 tumors showed an enhancing mass lesion at the right basal ganglia. On T_2 -weighted images, a wider area of high signal intensity was seen beyond the enhancing mass (Figure 5A, B). Compared with J3T-1 tumors, J3T-2 tumors exhibited a diffuse high signal intensity area in the right basal ganglia on T_2 -weighted images. There was no area of enhancement in these tumors (Figure 5C, D).

Survival of Mice Harboring J3T-1 and J3T-2 Brain Tumors

The cell doubling time of J3T-1 tumors was 19.5 hours and that of J3T-2 tumors was 17.4

hours. All athymic rats and mice inoculated with J3T-1 and J3T-2 developed brain tumors and died of tumor progression. The mean survival time of mice harboring J3T-1 ($n = 9$) and J3T-2 ($n = 8$) brain tumors was 33 days and 48 days, respectively (Figure 6).

Two Phenotypes of Invasion Were Concurrently Seen in Human Glioblastomas

To analyze invasion patterns in relation to vasculature and to correlate these patterns with animal data, dual immunohistochemical staining with glioma-specific antibody (MAP2e) and endothelial-specific antibody (vWf) was performed in five human glioblastoma samples. The degree of angiogenesis at the tumor borders, the degree of perivascular MAP2e-positive cell cuffing, and the density of single tumor cell infiltration in the cerebral cortex overlaying the tumor mass were determined (Table 2).

All glioma cells in each sample were positive for MAP2e. The center of the tumor comprised an area of high-density tumor cells. Furthermore, necrosis and

pseudopalisading glioma cells were seen in the core of the tumor (Figure 7E). Marked angiogenesis, which is characterized by thick endothelial proliferation, was seen in the center and at the tumor borders (Figure 7B). Furthermore, diffuse single cell infiltration from the tumor core to the surrounding healthy brain parenchyma (Figure 7D, G) was observed, thus rendering the border between the tumor and healthy brain tissue indistinct (Figure 7A). At the borders, clusters of MAP2e-positive cells were observed around dilated vessels in all cases (Figure 7C, F), despite some differences in the thickness of surrounding tumor cell layer, vessel density, and vessel diameter (Table 2). Cases 4 and 5 demonstrated fewer perivascular MAP2e-positive cells than cases 1 and 2. Infiltration by single cells distributed far beyond the area of cluster formation around new vessels. In distant areas, such as the cerebral cortex overlaying the tumor mass, scattered MAP2e-positive cells were also found in all cases; however, no dilated vessels or clusters of glioma cells around vessels were seen (Figure 7D, G).

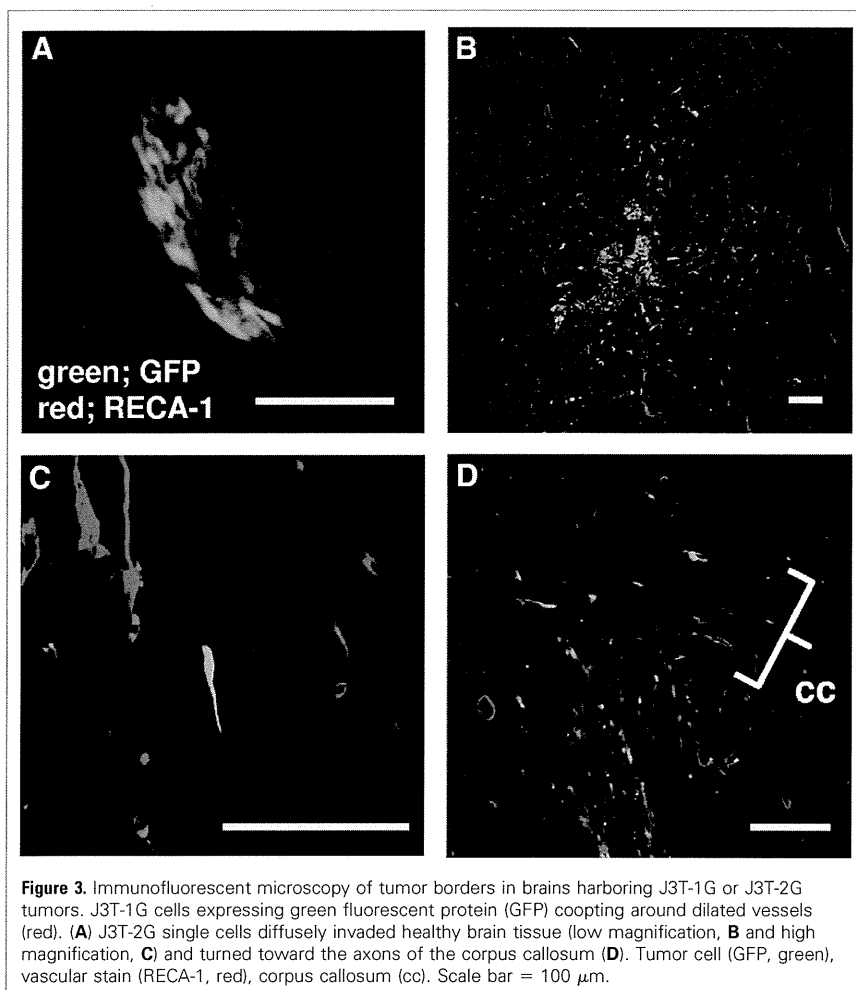


Figure 3. Immunofluorescent microscopy of tumor borders in brains harboring J3T-1G or J3T-2G tumors. J3T-1G cells expressing green fluorescent protein (GFP) coopting around dilated vessels (red). (A) J3T-2G single cells diffusely invaded healthy brain tissue (low magnification, B and high magnification, C) and turned toward the axons of the corpus callosum (D). Tumor cell (GFP, green), vascular stain (RECA-1, red), corpus callosum (cc). Scale bar = 100 μ m.

Molecular Profile of J3T-1 and J3T-2 Cells by Immunocytochemistry

VEGF and integrin $\alpha v \beta 3$ are well-studied key molecules in angiogenesis and invasion, respectively. Immunocytochemistry against VEGF and integrin $\alpha v \beta 3$ in J3T-1 and J3T-2 cells were examined (Figure 8). VEGF was shown to be overexpressed in J3T-1 cells, whereas J3T-2 cells showed no expression (Figure 8A, B). On the other hand, J3T-2 cells overexpressed protein of integrin $\alpha v \beta 3$ compared with J3T-1 cells (Figure 8C, D).

Molecular Profile of J3T-1 and J3T-2 Cells by Quantitative Reverse Transcription PCR

A summary of quantitative reverse transcription PCR data is shown in Figure 9. Gene expression of matrix metalloprotei-

nase-2 (MMP-2), nestin, and secreted protein acidic and rich in cysteine (SPARC) were higher in J3T-2 cells than in J3T-1 cells, whereas gene expression of matrix metalloproteinase-9 (MMP-9), hypoxia-inducible factor-1 (HIF-1), and platelet-derived growth factor (PDGF) were higher in J3T-1 cells than in J3T-2 cells.

DISCUSSION

Establishment of Novel Animal Glioma Models With Different Invasive Phenotypes

We have established two novel animal models with different invasive phenotypes and have compared their pathologic features with that of human glioblastoma samples.

First, we established two cell subclones from the same parental cell line. These re-

producibly established brain tumors with their inherent invasive phenotypes. It is possible that these differences in phenotype arose from differences in genotype. These genetic differences could have developed during culture in vitro due to genetic instability (35). J3T-1 cells formed densely packed, well-demarcated tumor mass with marked angiogenesis. In healthy parenchyma adjacent to the main tumor mass, clusters of tumor cells were seen with dilated blood vessels in them. In contrast, J3T-2 cells formed poorly demarcated tumors at the center. Diffuse infiltration by single cells was seen from the tumor center to the healthy brain parenchyma. These features, namely, perivascular cluster-forming invasion and single cell infiltration into healthy parenchyma, were specific for each cell line and did not overlap with each other.

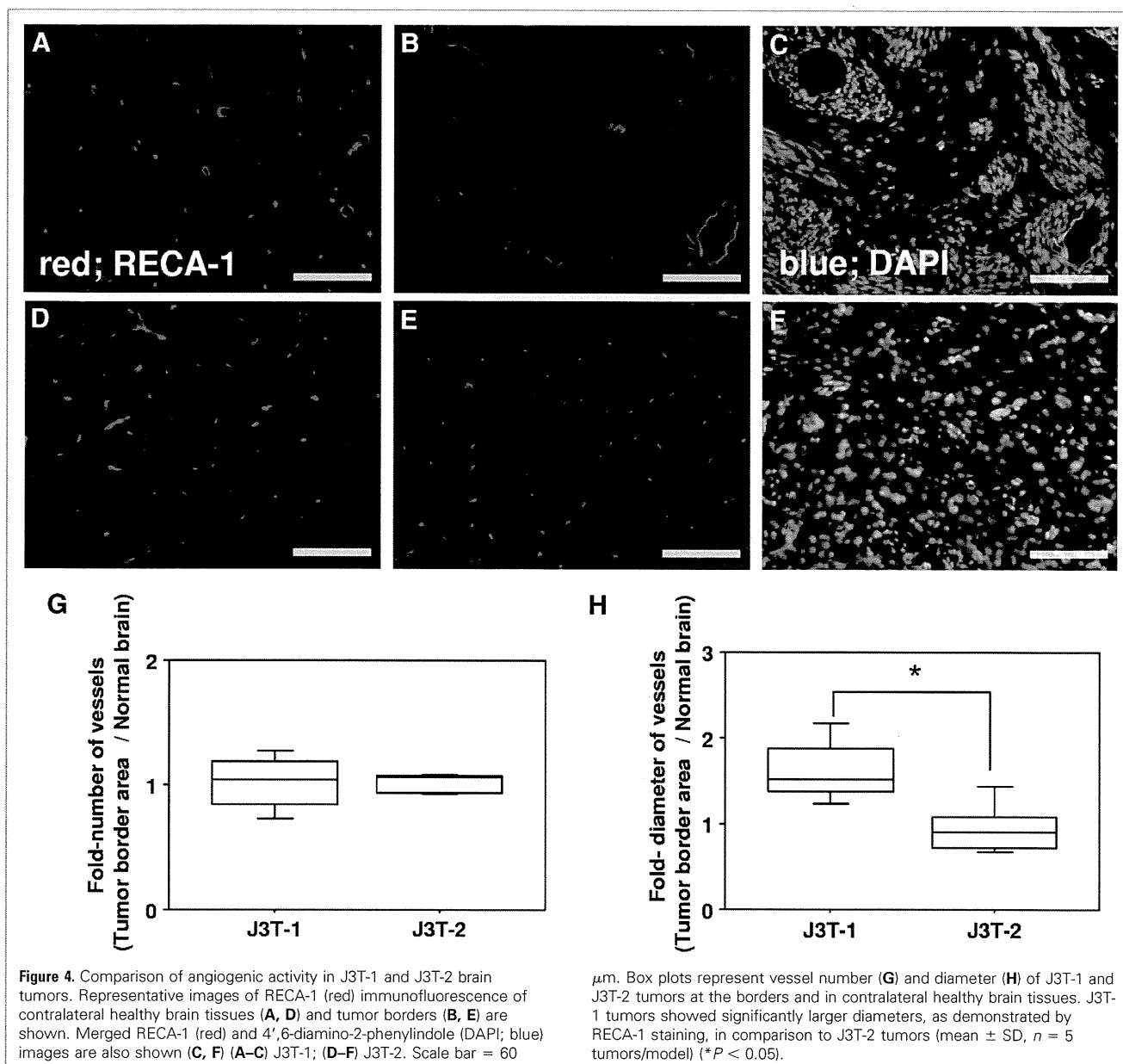
Second, we evaluated pathologic specimens of human glioblastoma and found that there were at least two invasive phenotypes: cluster formation around neovascular vessels, and single cell infiltration into healthy parenchyma.

On comparison of pathologic findings from experimental models and human glioblastoma samples, it was confirmed that each described animal glioma model represented the two phenotypes of human glioblastoma invasion.

The Two Invasive Phenotypes Are Angiogenesis-Dependent and Angiogenesis-Independent

Initially, we focused on tumor cell invasion, but found that invasion appears to be closely related to angiogenesis.

In animal models, J3T-1 was characterized by remarkable angiogenic activity and tumor cell cuffing around dilated vessels. In human samples, we found that tumor cell cuffing was only seen around dilated vessels with thickened epithelium in the marginal area, which is a characteristic of neovascular vessels (33). Therefore, we believe that tumor cells migrated along the abluminal surfaces of neovascular vessels and proliferated around them. Several investigators have reported similar findings in experimental models or in pathologic samples of human glioma (3, 11, 15). These reports showed glioma cell migration along vessels; however, these reports did not note the relationship between glioma cell invasion and angiogenesis. Holash et al. (23) re-



ported vascular cooption of glioma cells and angiogenesis in the development of experimental glioma. Many molecules are known to be related to the development of angiogenesis. By comparative profiling of these cell lines, we have shown that VEGF, MMP-9, HIF-1, and PDGF were overexpressed in J3T-1 cells than in J3T-2 cells. VEGF is one of most important diffusible angiogenic factor secreted by coopting tumor cells (45). Several mechanisms have been implicated in hypoxia-driven VEGF production. Activation of VEGF messenger

RNA transcription from DNA is mediated by binding of HIF-1. Autocrine or paracrine factors of the glioma microenvironment, PDGF, also contribute to the increased production of VEGF in gliomas (36). Raithatha et al. (38) reported that MMP-9 may regulate angiogenic remodeling. The endothelial cells stimulated by angiogenic factors then migrate and proliferate, resulting in neovascular formation (46). This paracrine loop leads to an extended foothold that allows tumor cells to migrate. As described previously, glioma cell cooption, perivascu-

lar migration, proliferation, and angiogenesis are closely related and progress concurrently (**Figure 10A**). Therefore, this invasive phenotype is exclusively angiogenesis-dependent. The evidence that no single cell infiltration independent of vasculature was seen in the J3T-1 brain tumor model is a paradoxical proof of this phenomenon.

The infiltrative pattern of the J3T-2 xenograft model was different from that of J3T-1. J3T-2 cells migrated singly to healthy parenchyma, independent of vasculature, and showed a tendency to migrate along my-

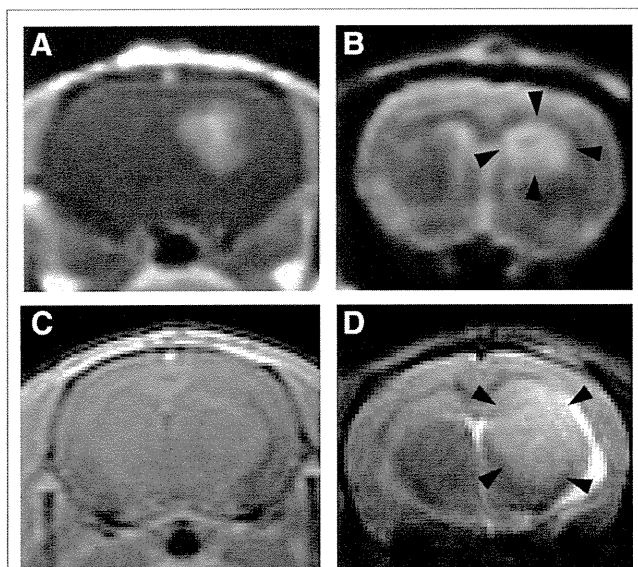


Figure 5. Magnetic resonance imaging coronal view of rat brains at the level of the largest lesion diameter. (A) Gadolinium-diethylenetriaminepenta-acetic acid (Gd-DTPA)-enhanced T_1 -weighted image of a rat J3T-1 tumor. (B) T_2 -weighted image of a rat J3T-1 tumor. (C) Gd-DTPA-enhanced T_1 -weighted image of a rat J3T-2 tumor. (D) T_2 -weighted image of a rat J3T-2 tumor. Note that the diffuse high signal intensity area (arrowheads) is depicted in both tumors on T_2 -weighted images (B, D); however, remarkable enhancement with Gd-DTPA is seen only for J3T-1 tumors (A) and not for J3T-2 tumors (C).

elinated axons in the corpus callosum and cortex. No dilated blood vessels or clusters of tumor cells were seen in areas of the tumor distant from the center. Similar mod-

els showing diffuse infiltration of glioma cells are rare. Recently, several investigative groups (2, 35, 40) have established diffusely invading gliomas from human glioma sam-

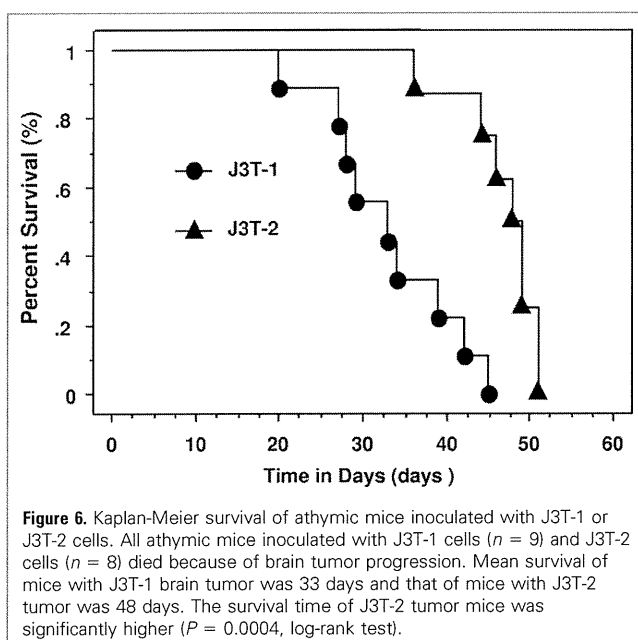


Figure 6. Kaplan-Meier survival of athymic mice inoculated with J3T-1 or J3T-2 cells. All athymic mice inoculated with J3T-1 cells ($n = 9$) and J3T-2 cells ($n = 8$) died because of brain tumor progression. Mean survival of mice with J3T-1 brain tumor was 33 days and that of mice with J3T-2 tumor was 48 days. The survival time of J3T-2 tumor mice was significantly higher ($P = 0.0004$, log-rank test).

ples. They also showed that such tumor models lack angiogenesis (35). In human samples, we found that most of the single cells did not seem to form clusters or did not adhere to distant vasculature. Few reports have referred to the infiltrative growth pattern of tumor cells following myelinated axons in histopathologic examination of human malignant glioma samples (3, 18, 41). Bernsen et al. (7) reported the complete absence of angiogenesis in samples of gliomatosis cerebri, which is an extreme example of such diffuse infiltrative growth of glial tumors. Therefore, this invasive phenotype was angiogenesis-independent and the foothold of tumor cells is mainly along myelinated axons (Figure 10B). By comparative profiling, we have shown that integrin $\alpha\beta_3$, MMP-2, nestin, and SPARC were overexpressed in J3T-2 cells than in J3T-1 cells. Integrin $\alpha\beta_3$ is expressed by tumor cells at the invasive edge of the tumor (3, 4). MMP-2 is known to be important in the invasive properties of neoplastic cells (3). The interaction of integrin $\alpha\beta_3$ with one of its ligands, vitronectin, may contribute to invasion by regulating the activation of proteases, including MMP-2 (3, 4, 12). SPARC promotes brain tumor invasion in vivo and in in vitro study (42). MMP-2 expression is up-regulated by SPARC using cDNA array analysis in U87T2 and A2b2 clones (19). Nestin is an intermediate filament protein, commonly used as a marker for undifferentiated cells in the developing CNS and for CNS tumors. Kitai et al. (29) reported that nestin is a useful marker for examining the infiltration of malignant astrocytic cells into surrounding tissue.

Results from MRI studies support the interpretation of the angiogenic status of the two animal models. In human malignant glioma, gadolinium enhancement was seen in the main mass where the blood-brain barrier (BBB) of neovascular vessels was disrupted. Diffuse astrocytoma or gliomatosis cerebri were characterized by diffuse high intensity lesions on T_2 -weighted images and absence of enhancement on T_1 -weighted images. The diffuse invasive area around the enhancing mass of a malignant glioma was also depicted as high intensity on T_2 -weighted images (47). Therefore, angiogenesis was observed only in J3T-1 tumors that showed gadolinium enhancement due to BBB disruption, and not in J3T-2 tumors.

Table 2. Immunohistochemical Analysis of Two Types of Invasion in Human Glioblastoma Samples

Case	Age/Sex	Degree of Angiogenesis at the Tumor Border	Degree of Perivascular MAP2e-positive Cell Cuffing	Density of Single Tumor Cell in Cerebral Cortex
1	69/M	+++	+++	+++
2	67/M	+++	+++	+++
3	76/M	++	++	+++
4	58/M	+	+	+++
5	75/M	+	+	+++

Histopathologic examination of the experimental animal models and human glioblastoma samples confirmed that there were at least two invasive and angiogenic phenotypes, namely angiogenesis-dependent and angiogenesis-independent invasion. Therefore, angiogenesis was an important factor contributing to the regulation of patterns of invasion.

Examination of human tumor samples demonstrated that malignant astrocytoma and glioblastoma consisted of a mixture of subclones that showed angiogenesis-dependent and angiogenesis-independent invasion in various proportions. In addition, gliomatosis cerebri is an extreme example of a tumor developed solely by subclones that show angiogenesis-independent invasion.

Importance of Both Invasion and Angiogenesis as Targets in Treating Malignant Gliomas

Currently available therapeutic agents for malignant glioma are mostly antiproliferative and antiangiogenic agents.

Antiproliferative drugs can be delivered to tumor cells in the center and at the margins of tumors through BBB-disrupted neo-

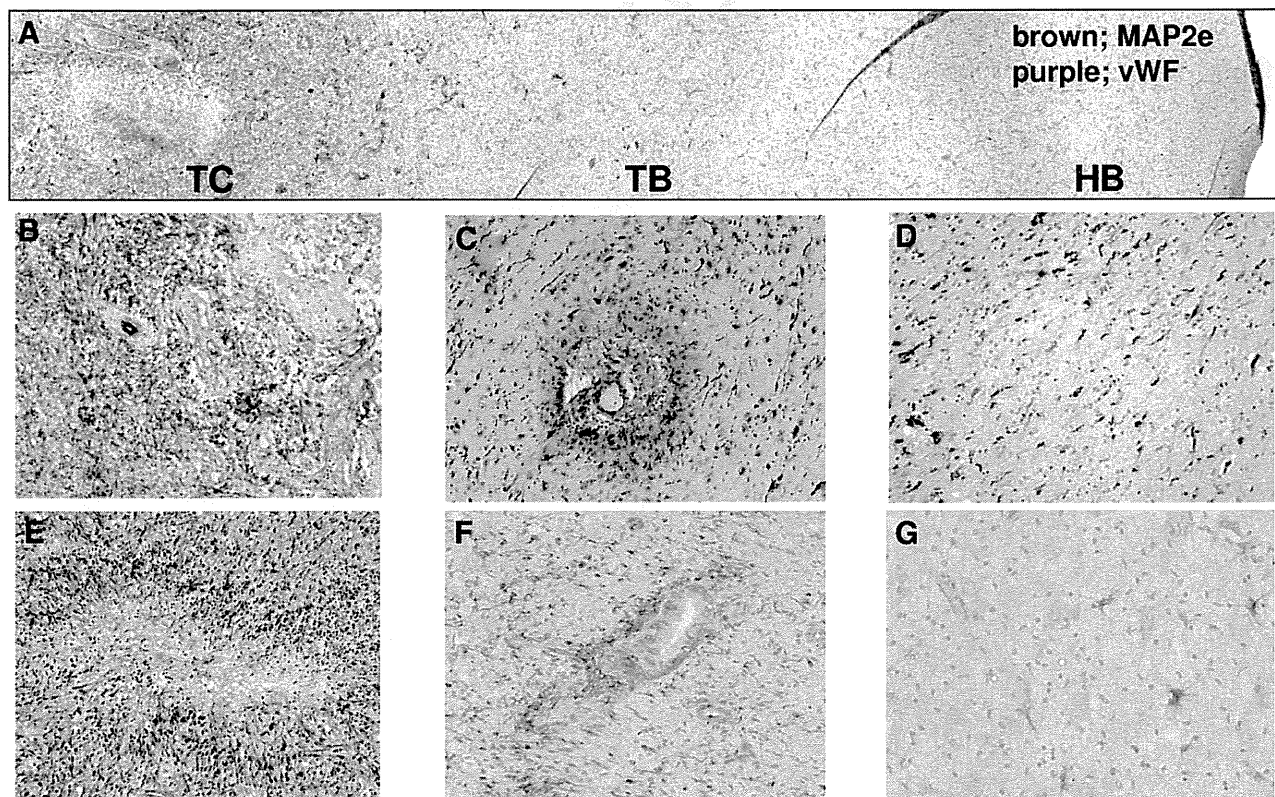
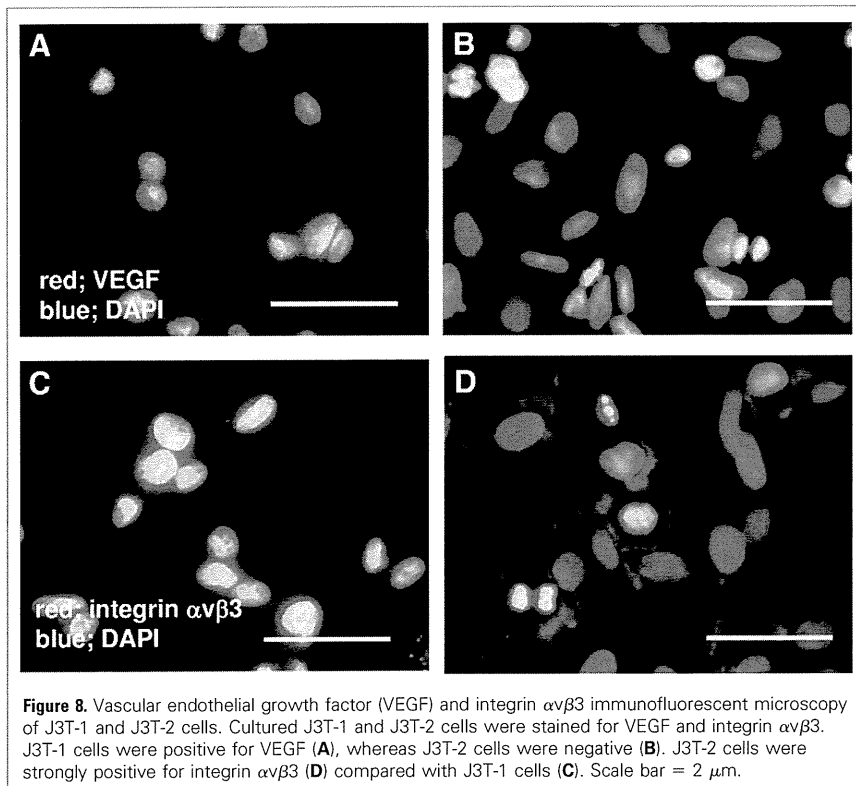


Figure 7. MAP2e and vWf immunohistochemical staining of human glioblastoma samples. Macroscopic appearance of glioblastoma samples in case 2 (A). Tumor cells diffusely infiltrated from the tumor center (TC) to the healthy brain (HB) tissue; there is no border between them. TC showed high tumor cell density, endothelial proliferation (B, case 3), and pseudopalisading of tumor cells around the necrotic focus (E, case 1). At

the tumor border (TB), MAP2e-positive tumor cells clustered around dilated vessels (C, case 5; F, case 1). In HB tissues, single MAP2e-positive tumor cells were diffusely distributed; however, no dilated vessels were observed (D, case 1; G, case 2). MAP2e, DAB; vWf, DAB-Ni; counterstain, hematoxylin; TC, tumor center; TB, tumor border; HB, healthy brain.



vascular vessels; however, most drugs cannot reach diffusely infiltrating tumor cells that are angiogenesis-independent. Re-

cently, temozolomide has been reported as the most effective anti-glioma agent; however, not all of the cells in gliomas are de-

stroyed by temozolomide and patient cure has not been achieved. Antiproliferative agents, such as temozolomide, do not have anti-invasive activity, and thus result in treatment failure.

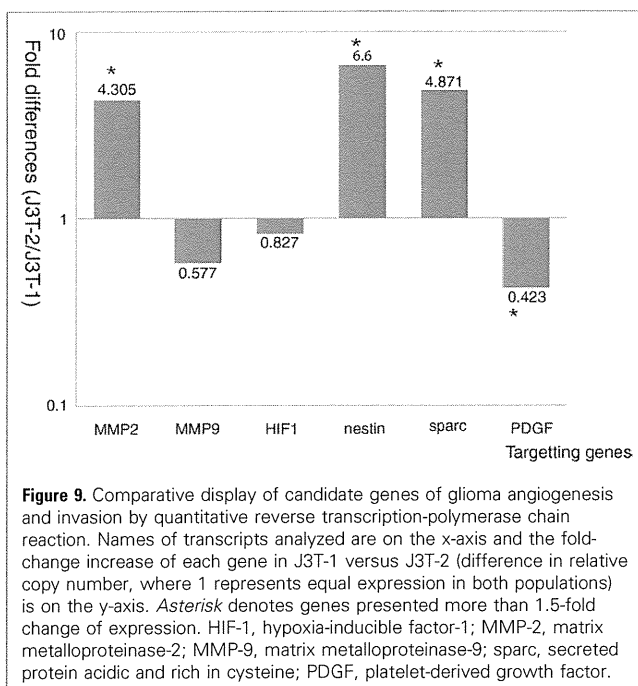
Recent data showing the clinical use of antiangiogenic drugs for recurrent malignant gliomas have been disappointing (37). Some patients treated with bevacizumab, a humanized monoclonal antibody against VEGF, have shown regression of gadolinium-enhancing main tumors, but significant increases in the volume of infiltrative tumor relative to the enhancing tumor were also observed. Similar results have been reported in clinical settings and experimental models (30, 39, 48).

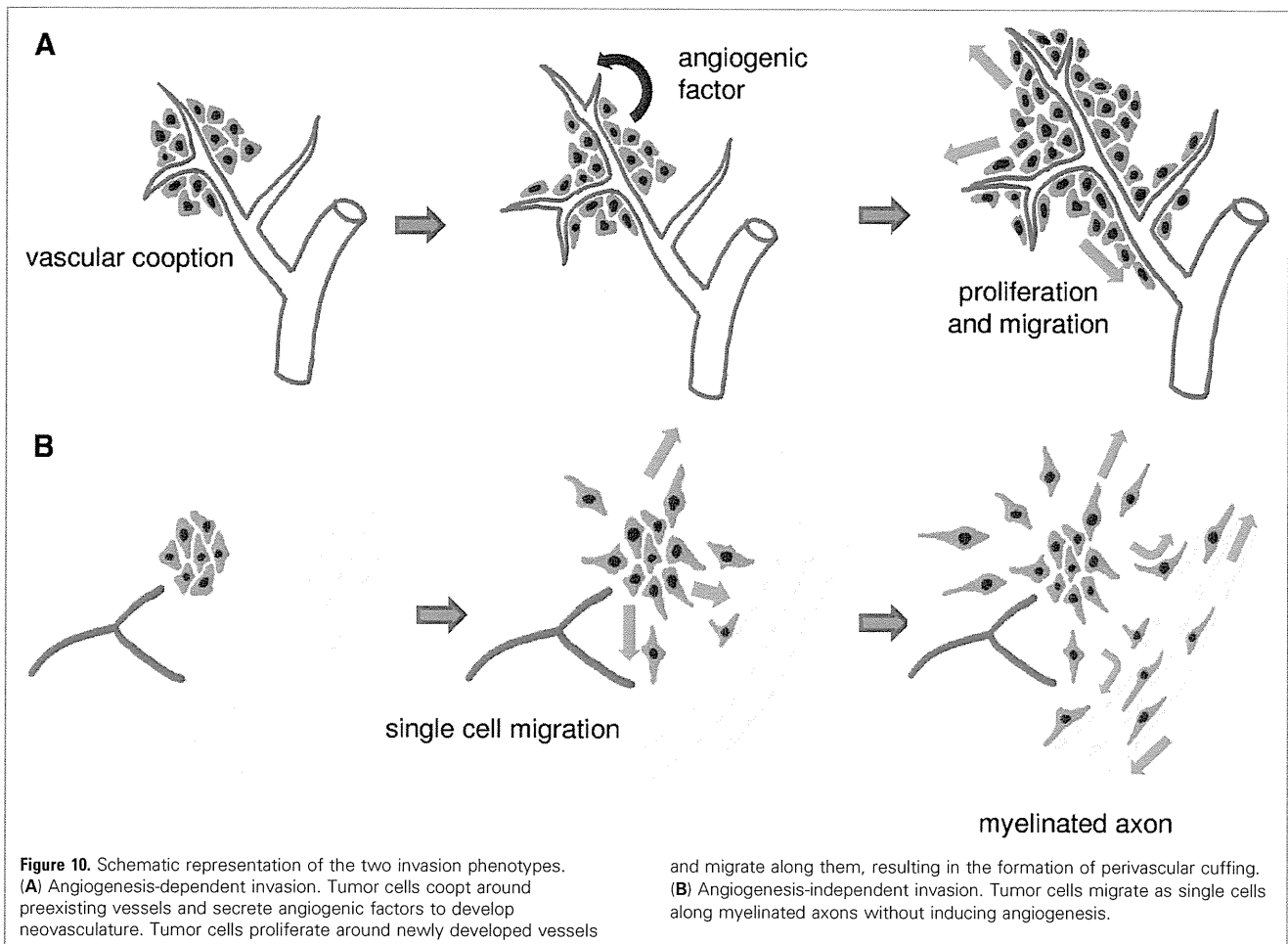
According to our results, most of the malignant glioma originally consisted of both phenotypes of tumor cells. Therefore, these chemotherapies may affect only glioma cells with angiogenesis-dependent invasion and not those with angiogenesis-independent invasion and may even lead to a switch in the dominant invasion pattern from angiogenesis-dependent to angiogenesis-independent. As mentioned previously, these distinct invasive patterns complicate curative treatment, and hence, must be distinguished to develop novel approaches for human glioma therapy. Curative treatment of gliomas should target cells with both angiogenesis-dependent and angiogenesis-independent invasion concurrently. Our animal models facilitated their identification, and thereby, the development of novel therapeutic strategies such as oncolytic viruses, tumor-targeted stem cell, or immunotherapy (24, 26, 28, 31).

Usefulness of our Models for Molecular Analysis and Experimental Therapy

J3T-1 and J3T-2 brain tumor models provide a reproducible in vitro and in vivo system to study the mechanisms of invasion and angiogenesis of gliomas. There are several advantages to our novel animal models.

First, J3T-1 and J3T-2 brain tumor models are the exclusive cell line-based invasive animal models. Traditional animal models of glioma have been criticized for not recapitulating the main pathologic features of human glioma (13). They developed a well-demarcated tumor mass at the inoculation site, but did not aggressively invade healthy brain tissue. Recently, some animal models have been reported in which human glioma





xenografts showed various degrees of diffuse invasion (10, 14, 16, 17, 21, 25, 50). However, these models required some special procedures to establish brain tumors, such as *in vivo* preparation of xenografts or *in vitro* spheroid formation before implantation (10, 20, 34, 50). They cost and need more time than cell line-based animal models. Another disadvantage of these models was that tumors grew slowly, and thus, required a long observation period. Compared with these models, our cell line-based models can be established easily with uncomplicated cell preparations and they have shown stable reproducibility of tumor development as well as the same phenotypic growth shown in human glioma. The moderate survival time of the animals is also suitable for experimental assessment. In addition, there is a potential utility of these cells to establish invasive glioma models in immunocompetent canines. Berens et al.

(6) established allogeneic brain tumor model in immunocompetent canine. Candolfi et al. (8, 9) reported that spontaneous canine glioblastoma very closely approximate the human disease relative to histopathology, epidemiology, and clinical course. Because the canine glioma model is the only large animal model available, this would be more useful for establishing novel therapies to optimize treatment schedule and to assess immune response or therapy-related toxicity.

Second, the most significant advantage of our models is that they are a pair of sibling subclones that show different phenotypes *in vivo*, but have a similar genetic background. Similarity in genotype but difference in phenotype makes our models suitable for comparative study of genetic or proteomic profiles to narrow down molecular fluctuations between the types in experimental settings. Molecular materials

for canine cells are limited; however, some microarrays or antibodies are commercially available. Therefore, our model is suitable for molecular analysis to elucidate the mechanisms of glioma invasion. We have shown molecular profiles of these cell lines that may regulate each phenotypes of invasion by comparative analysis of gene or protein expression between subclones J3T-1 and J3T-2. Furthermore, results of *in vitro* analysis can be directly verified *in vivo* using our animal models.

Third, animals harboring J3T-1 or J3T-2 brain tumors die of tumor progression. Therefore, these animal models are suitable for the assessment of experimental treatments. The lack of glioma models that mimic the pathologic condition of human glioma has been responsible, in some part, for the failure of conventional therapy. Models that especially reflect invasive phe-

notypes are absolutely necessary for the development and evaluation of novel therapeutic approaches.

CONCLUSIONS

In the present study we have established two new cell line-based animal models of invasive glioma. Each of our animal models, J3T-1 and J3T-2, histologically recapitulated two invasive and angiogenic phenotypes, namely angiogenesis-dependent and angiogenesis-independent invasion, also observed in human glioblastoma. Molecular profiles of these cell lines, which may regulate each phenotype of invasion, were shown by comparative analysis of gene or protein expression between two subclones. This unique pair of cell lines provided a reproducible in vitro and in vivo system to analyze the mechanisms of invasion and angiogenesis in glioma progression.

ACKNOWLEDGMENTS

We thank Hideki Wakimoto, Masako Arao, and Akina Ishikawa for their technical assistance. The following medical students also contributed animal experiments: Tetsuo Oka, Keiko Tanaka, Hiroyuki Honda, Ken Seno, Hiroko Okura, Tomoyo Mifune, and Satoshi Murai.

REFERENCES

- Barth RF, Kaur B: Rat brain tumor models in experimental neuro-oncology: the c6, 9l, t9, rg2, fg8, bt4c, rt-2 and cns-1 gliomas. *J Neurooncol* 94:299-312, 2009.
- Beier D, Hau P, Proescholdt M, Lohmeier A, Wischhusen J, Oefner PJ, Aigner L, Brawanski A, Bogdahn U, Beier CP: Cdr133(+) and cdr133(-) glioblastoma-derived cancer stem cells show differential growth characteristics and molecular profiles. *Cancer Res* 67:4010-4015, 2007.
- Bellail AC, Hunter SB, Brat DJ, Tan C, Van Meir EG: Microregional extracellular matrix heterogeneity in brain modulates glioma cell invasion. *Int J Biochem Cell Biol* 36:1046-1069, 2004.
- Bello L, Francolini M, Marthyn P, Zhang J, Carroll RS, Nikas DC, Strasser JF, Villani R, Cheresch DA, Black PM: Alpha(v)beta3 and alpha(v)beta5 integrin expression in glioma periphery. *Neurosurgery* 49:380-389 [discussion: 390], 2001.
- Berens ME, Bjotvedt G, Levesque DC, Rief MD, Shapiro JR, Coons SW: Tumorigenic, invasive, karyotypic, and immunocytochemical characteristics of clonal cell lines derived from a spontaneous canine anaplastic astrocytoma. *In Vitro Cellular & Developmental Biology-Animal* 29:310-318, 1993.
- Berens ME, Giese A, Shapiro JR, Coons SW: Allogeneic astrocytoma in immune competent dogs. *Neoplasia* 1:107-112, 1999.
- Bernsen H, Van der Laak J, Kusters B, Van der Ven A, Wesseling P: Gliomatosis cerebri: quantitative proof of vessel recruitment by cooption instead of angiogenesis. *J Neurosurg* 103:702-706, 2005.
- Candolfi M, Curtin JF, Nichols WS, Muhammad AG, King GD, Pluhar GE, McNiel EA, Ohlfest JR, Freese AB, Moore PF, Lerner J, Lowenstein PR, Castro MG: Intracranial glioblastoma models in pre-clinical neuro-oncology: neuropathological characterization and tumor progression. *J Neurooncol* 85:133-148, 2007.
- Candolfi M, Pluhar GE, Kroeger K, Puntel M, Curtin J, Barcia C, Muhammad AKM, Xiong W, Liu C, Mondkar S: Optimization of adenoviral vector-mediated transgene expression in the canine brain in vivo, and in canine glioma cells in vitro. *Neuro-Oncology* 9:245-258, 2007.
- Claes A, Wesseling P, Jeuken J, Maass C, Heerschap A, Leenders WP: Antiangiogenic compounds interfere with chemotherapy of brain tumors due to vessel normalization. *Mol Cancer Ther* 7:71-78, 2008.
- Cretu A, Fotos JS, Little BW, Galileo DS: Human and rat glioma growth, invasion, and vascularization in a novel chick embryo brain tumor model. *Clin Exp Metastasis* 22:225-236, 2005.
- Demuth T, Berens ME: Molecular mechanisms of glioma cell migration and invasion. *J Neurooncol* 70:217-228, 2004.
- Ding H, Nagy A, Gutmann DH, Guha A: A review of astrocytoma models. *Neurosurg Focus* 8:1-8, 2000.
- Engelbraaten O, Hjortland GO, Hirschberg H, Fodstad O: Growth of precultured human glioma specimens in nude rat brain. *J Neurosurg* 90:125-132, 1999.
- Farin A, Suzuki SO, Weiker M, Goldman JE, Bruce JN, Canoll P: Transplanted glioma cells migrate and proliferate on host brain vasculature: a dynamic analysis. *Glia* 53:799-808, 2006.
- Galli R, Binda E, Orfanelli U, Cipelletti B, Gritti A, De Vitis S, Fiocco R, Foroni C, Dimeco F, Vescovi A: Isolation and characterization of tumorigenic, stem-like neural precursors from human glioblastoma. *Cancer Res* 64:7011-7021, 2004.
- Giannini C, Sarkaria JN, Saito A, Uhm JH, Galanis E, Carlson BL, Schroeder MA, James CD: Patient tumor egrf and pdgfra gene amplifications retained in an invasive intracranial xenograft model of glioblastoma multiforme. *Neuro Oncol* 7:164-176, 2005.
- Giese A, Bjerkvig R, Berens ME, Westphal M: Cost of migration: invasion of malignant gliomas and implications for treatment. *J Clin Oncol* 21:1624-1636, 2003.
- Golembieski WA, Rempel SA: Cdna array analysis of sparc-modulated changes in glioma gene expression. *J Neurooncol* 60:213-226, 2002.
- Goplen D, Wang J, Enger PO, Tysnes BB, Terzis AJA, Laerum OD, Bjerkvig R: Protein disulfide isomerase expression is related to the invasive properties of malignant glioma. *Cancer Res* 66:9895-9902, 2006.
- Gunther HS, Schmidt NO, Phillips HS, Kemming D, Kharbanda S, Soriano R, Modrusan Z, Meissner H, Westphal M, Lamszus K: Glioblastoma-derived stem cell-enriched cultures form distinct subgroups according to molecular and phenotypic criteria. *Oncogene* 27:2897-2909, 2008.
- Hampf JA, Camp SM, Mydlarz WK, Hampl M, Ichikawa T, Chiocca EA, Louis DN, Sena-Esteves M, Breakefield XO: Potentiated gene delivery to tumors using herpes simplex virus/epstein-barr virus/rv tribrid amplicon vectors. *Hum Gene Ther* 14:611-626, 2003.
- Holash J, Maisonpierre PC, Compton D, Boland P, Alexander CR, Zagzag D, Yancopoulos GD, Wiegand SJ: Vessel cooption, regression, and growth in tumors mediated by angiotensins and vegf. *Science* 284:1994, 1999.
- Hong X, Miller C, Savant-Bhonsale S, Kalkanis SN: Antitumor treatment using interleukin-12-secreting marrow stromal cells in an invasive glioma model. *Neurosurgery* 64:1139-1146 [discussion: 1146-1147], 2009.
- Horten BC, Basler GA, Shapiro WR: Xenograft of human malignant glial tumors into brains of nude mice. A histopathological study. *J Neuropathol Exp Neurol* 40:493-511, 1981.
- Ichikawa T, Chiocca EA: Comparative analyses of transgene delivery and expression in tumors inoculated with a replication-conditional or -defective viral vector. *Cancer Res* 61:5336-5339, 2001.
- Ichikawa T, Tamiya T, Adachi Y, Ono Y, Matsumoto K, Furuta T, Yoshida Y, Hamada H, Ohmoto T: In vivo efficacy and toxicity of 5-fluorocytosine/cytosine deaminase gene therapy for malignant gliomas mediated by adenovirus. *Cancer Gene Ther* 7:74-82, 2000.
- Kambara H, Okano H, Chiocca EA, Saeki Y: An oncolytic hsv-1 mutant expressing icp34.5 under control of a nestin promoter increases survival of animals even when symptomatic from a brain tumor. *Cancer Res* 65:2832-2839, 2005.
- Kitai R, Horita R, Sato K, Yoshida K, Arishima H, Higashino Y, Hashimoto N, Takeuchi H, Kubota T, Kikuta K: Nestin expression in astrocytic tumors delineates tumor infiltration. *Brain Tumor Pathol* 27:17-21, 2010.
- Kunkel P, Ulbricht U, Bohlen P, Brockmann MA, Fillbrandt R, Stavrou D, Westphal M, Lamszus K: Inhibition of glioma angiogenesis and growth in vivo by systemic treatment with a monoclonal antibody against vascular endothelial growth factor receptor-2. *Cancer Res* 61:6624-6628, 2001.
- Kurozumi K, Hardcastle J, Thakur R, Yang M, Christoforidis G, Fulci G, Hochberg FH, Weissleder R, Carson W, Chiocca EA, Kaur B: Effect of tumor

- microenvironment modulation on the efficacy of oncolytic virus therapy. *J Natl Cancer Inst* 99:1768-1781, 2007.
32. Lakka SS, Gondi CS, Yanamandra N, Olivero WC, Dinh DH, Gujrati M, Rao JS: Inhibition of cathepsin b and mmp-9 gene expression in glioblastoma cell line via RNA interference reduces tumor cell invasion, tumor growth and angiogenesis. *Oncogene* 23:4681-4689, 2004.
 33. Louis DN, Ohgaki H, Wiestler OD, Cavenee WK, Burger PC, Jouvet A, Scheithauer BW, Kleihues P: Glioblastoma. In: WHO Classification of Tumours of the Central Nervous System. vol 2. Lyon: IARC; 2007:33-49.
 34. Mahesparan R, Read TA, Lund-Johansen M, Skafnesmo K, Bjerkvig R, Engebraaten O: Expression of extracellular matrix components in a highly infiltrative in vivo glioma model. *Acta Neuropathologica* 105:49-57, 2003.
 35. Martens T, Laabs Y, Gunther HS, Kemming D, Zhu Z, Witte L, Hagel C, Westphal M, Lamszus K: Inhibition of glioblastoma growth in a highly invasive nude mouse model can be achieved by targeting epidermal growth factor receptor but not vascular endothelial growth factor receptor-2. *Clin Cancer Res* 14:5447-5458, 2008.
 36. Mentlein R, Held-Feindt J: Angiogenesis factors in gliomas: a new key to tumour therapy? *Naturwissenschaften* 90:385-394, 2003.
 37. Norden AD, Young GS, Setayesh K, Muzikansky A, Klufas R, Ross GL, Ciampa AS, Ebbeling LG, Levy B, Drappatz J: Bevacizumab for recurrent malignant gliomas: efficacy, toxicity, and patterns of recurrence. *Neurology* 70:779-787, 2008.
 38. Raithatha SA, Muzik H, Muzik H, Rewcastle NB, Johnston RN, Edwards DR, Forsyth PA: Localization of gelatinase-a and gelatinase-b mRNA and protein in human gliomas. *Neuro Oncol* 2:145-150, 2000.
 39. Rubenstein JL, Kim J, Ozawa T, Zhang M, Westphal M, Deen DF, Shuman MA: Anti-vegf antibody treatment of glioblastoma prolongs survival but results in increased vascular cooption. *Neoplasia* 2:306-314, 2000.
 40. Sakariassen PO, Prestegarden L, Wang J, Skafnesmo KO, Mahesparan R, Molthoff C, Sminia P, Sundlisaeter E, Misra A, Tysnes BB, Chekenya M, Peters H, Lende G, Kalland KH, Oyan AM, Petersen K, Jonassen I, van der Kogel A, Feuerstein BG, Terzis AJ, Bjerkvig R, Enger PO: Angiogenesis-independent tumor growth mediated by stem-like cancer cells. *Proc Natl Acad Sci U S A* 103:16466-16471, 2006.
 41. Scherer HJ: The forms of growth in gliomas and the practical significance. *Brain* 63:1-35, 1940.
 42. Schultz C, Lemke N, Ge S, Golembieski WA, Rempel SA: Secreted protein acidic and rich in cysteine promotes glioma invasion and delays tumor growth in vivo. *Cancer Res* 62:6270-6277, 2002.
 43. Stupp R, Hegi ME, Mason WP, van den Bent MJ, Taphoorn MJ, Janzer RC, Ludwin SK, Allgeier A, Fisher B, Belanger K, Hau P, Brandes AA, Gijtenbeek J, Marosi C, Vecht CJ, Mokhtari K, Wesseling P, Villa S, Eisenhauer B, Gorlia T, Weller M, Lacombe D, Cairncross JG, Mirimanoff RO: Effects of radiotherapy with concomitant and adjuvant temozolomide versus radiotherapy alone on survival in glioblastoma in a randomised phase III study: 5-year analysis of the EORTC-NCIC trial. *Lancet Oncol* 10:459-466, 2009.
 44. Suzuki SO, Kitai R, Llena J, Lee SC, Goldman JE, Shafit-Zagardo B: Map-2e, a novel map-2 isoform, is expressed in gliomas and delineates tumor architecture and patterns of infiltration. *J Neuropathol Exper Neurol* 61:403-412, 2002.
 45. Takano S, Yamashita T, Ohneda O: Molecular therapeutic targets for glioma angiogenesis. *J Oncol* 2010:351908, 2010.
 46. Tate MC, Aghi MK: Biology of angiogenesis and invasion in glioma. *Neurotherapeutics* 6:447-457, 2009.
 47. Tovi M, Hartman M, Lilja A, Ericsson A: MR imaging in cerebral gliomas. Tissue component analysis in correlation with histopathology of whole-brain specimens. *Acta Radiol* 35:495-505, 1994.
 48. Tuettenberg J, Friedel C, Vajkoczy P: Angiogenesis in malignant glioma? A target for antitumor therapy? *Crit Rev Oncol Hematol* 59:181-193, 2006.
 49. Tysnes BB, Mahesparan R: Biological mechanisms of glioma invasion and potential therapeutic targets. *J Neurooncol* 53:129-147, 2001.
 50. Wang J, Miletic H, Sakariassen PO, Huszthy PC, Jacobsen H, Brekka N, Li X, Zhao P, Mork S, Chekenya M, Bjerkvig R, Enger PO: A reproducible brain tumour model established from human glioblastoma biopsies. *BMC Cancer* 9:465, 2009.

Conflict of interest statement: This study was supported by grants-in-aid for Scientific Research from the Japanese Ministry of Education, Culture, Sports, Science, and Technology to Tomotsugu Ichikawa (19591675), Hirokazu Kambara (19591676), and Kazuhiko Kurozumi (20890133 and 21791364).

received 28 February 2011; accepted 02 September 2011

Citation: World Neurosurg. (2012).

DOI: 10.1016/j.wneu.2011.09.005

Journal homepage: www.WORLDNEUROSURGERY.org

Available online: www.sciencedirect.com

1878-8750/\$ - see front matter © 2012 Elsevier Inc.

All rights reserved.

Enhanced internalization of ErbB2 in SK-BR-3 cells with multivalent forms of an artificial ligand

Arun Vaidyanath^a, Toshihiro Hashizume^a, Tadahiro Nagaoka^{a, b}, Nao Takeyasu^a,
Hitomi Satoh^a, Ling Chen^a, Jiyou Wang^a, Tomonari Kasai^a, Takayuki Kudoh^a,
Ayano Satoh^c, Li Fu^d, Masaharu Seno^{a, *}

^a Laboratory of Nano-Biotechnology, Department of Medical Bioengineering Science,
Graduate School of Natural Science and Biotechnology, Okayama University, Kita-ku, Okayama, Japan

^b Tumour Growth Factor Section, Mammary Biology and Tumorigenesis Laboratory, Center for Cancer Research,
National Cancer Institute, Bethesda, MD, USA

^c Research Core for Interdisciplinary Sciences, Okayama University, Kita-ku, Okayama, Japan

^d Department of Breast Cancer Pathology and Research Laboratory, State Key Laboratory of Breast Cancer Research,
Cancer Hospital of Tianjin Medical University, Tianjin, China

Received: September 3, 2010; Accepted: January 4, 2011

Abstract

Targeting and down-regulation of ErbB2, a member of EGF receptor family, is regarded as one of the key aspect for cancer treatment because it is often overexpressed in breast and ovarian cancer cells. Although natural ligands for ErbB2 have not been found, unlike other ErbB receptors, EC-1, a 20-amino acid circular peptide, has been shown to bind to ErbB2 as an artificial ligand. Previously we showed EC-1 peptide did not induce the internalization of ErbB2 in SK-BR-3 cells. In this report, we designed divalent and multivalent forms of EC-1 peptide with the Fc portion of the human IgG and bionanocapsule modified with ZZ-tag on its surface to improve the interaction with ErbB2. These forms showed higher affinity to ErbB2 than that of EC-1 monomer. Furthermore, prominent endosomal accumulation of ErbB2 occurred in SK-BR-3 cells when stimulated with EC-Fc ligand multivalently displayed on the surface of the bionanocapsule, whereas SK-BR-3 cells as themselves displayed stringent mechanism against ErbB2 internalization without stimulation. The multivalent form of EC-1 peptide appeared to internalize ErbB2 more efficiently than divalent form did. This internalization was unaffected by the inhibition of clathrin association, but inhibited when the cholesterol was depleted which explained either caveolar or GPI-AP-early endocytic compartment (GEEC) pathway. Because of the lack of caveolin-1 expression, caveolar machinery may be lost in SK-BR-3 cell line. Therefore, it is suggested that the multivalent form of EC-1 induces the internalization of ErbB2 through the GEEC pathway.

Keywords: ErbB2 • EC-1 peptide • internalization • multivalent display • bionanocapsule

Introduction

The epidermal growth factor receptor (EGFR) family consisting of ErbB1 (EGFR), ErbB2, ErbB3 and ErbB4 is known to play a crucial part in the development and progression of cancers. The signal for cell survival, differentiation and proliferation is achieved through both homo- and heterodimerization of the receptors [1, 2].

Anomalous increase in the expression of the ErbB2 is an identified factor for the development of several cancer types [1, 3] and high ErbB2 levels parallel the worse prognosis for breast cancer patients [4–6]. ErbB2 also associates with ErbB3 in the hetero dimerization and is considered the most active dimer that initiates cancers [7, 8]. ErbB2 is overexpressed in breast (30%) and ovarian (15–30%) cancer [9–11]. The myriad roles played by ErbB2 have made it one of the most preferred targets for the treatment of cancer. ErbB2 stringently internalizes efficiently recruiting back to the cell surface [12]. The mechanism of ErbB2 recycling and degradation is complex and appears to vary depending on the cell types. Various groups have shown that geldanamycin treatment efficiently internalizes the ErbB2 ligand [13–15]. Although the

*Correspondence to: Masaharu SENO,
Faculty of Engineering, Okayama University,
Room 361, Building ENG-6, 3.1.1 Tsushima-Naka,
Kita-ku, Okayama 700-8530, Japan.
Tel.: +81-86-251-8216
Fax: +81-86-251-8216
E-mail: mseno@cc.okayama-u.ac.jp

internalization of ErbB2 is enhanced when multivalently cross-linked with antibody such as anti-ErbB2 antibody sc-08 [13, 16–19], there is no known natural ligand that promotes the ErbB2 internalization till date. By phage display method, small peptides, which possess binding affinity to ErbB2, have been isolated [20–22]. EC-1 peptide, a cyclic 20-amino-acid-peptide, is also one of the artificial ErbB2 ligands isolated from random peptide library of phage display [23]. EC-1 peptide is considered to abolish the tyrosine phosphorylation of the intracellular domain of ErbB2 and to inhibit the proliferation of SK-BR-3 cells overexpressing ErbB2.

Previously, EC-1 peptide fused to GFP was shown to stimulate internalization of ErbB2 in SK-OV-3 cells whereas ErbB2 in SK-BR-3 cells retained on the surface [24]. Because anti-ErbB2 antibody sc-08 stimulated the internalization of ErbB2 in both cell lines, the mechanism of internalization stimulated by EC-1 peptide was considered quite different from that by anti-ErbB2 antibody sc-08. In this study, we designed multivalent form using EC-1 peptide fused to human IgG-Fc domain (EC-Fc) and bionanocapsule displaying ZZ-tag on the surface [25]. We then asked whether the multivalent forms stimulated the internalization of ErbB2 in SK-BR-3 cells.

Materials and methods

Cell cultures

Human breast carcinoma derived cell lines, MCF-7, MDA-MB-453 and SK-BR-3, and human ovarian carcinoma cell line SK-OV-3 were from the ATCC (VA). SK-BR-3 and SK-OV-3 cells were grown at 37°C in RPMI-1640 medium supplemented with 10% FBS and MCF-7 in DMEM medium supplemented with 10% FBS under an atmosphere of 5% CO₂ and MDA-MB-453 cells in Leibovitz's L-15 medium supplemented with 10% FBS without conditioning CO₂. All culture media were supplemented with 2 mM glutamine just before use.

Construction of expression plasmids

The expression plasmid for EC-Fc was constructed as follows. The DNA fragment coding human IgG-Fc domain was excised from the plasmid pB0593 [26] with restriction enzymes AgeI and NotI and then ligated at the 3'-end of a synthetic oligonucleotide coding for the EC-1 peptide. The resultant sequence coding EC-Fc was ligated to the 3'-end of the sequence coding the signal peptide derived from human RNase1 [27]. Finally, the sequence coding EC-Fc with a secretion signal peptide was cloned downstream of CMV promoter to construct the plasmid pB0854 with hygromycin resistant gene. Simultaneously, the expression vector for Fc domain without EC-1 moiety was constructed in the same procedure to construct the plasmid pB0853.

Preparation of EC-Fc protein

Chinese hamster ovary (CHO) cells were transfected with the expression plasmid pB0854 for EC-Fc protein. The transformed cells were cultured in the presence of 100 µg/ml Hygromycin B (Wako Pure-Chemicals, Osaka,

Japan) for several weeks and cells stably expressing EC-Fc were pooled. Ten million of the transformed cells were seeded in 500 ml of CHO-S-SFMII (GIBCO, Carlsbad, CA, USA) containing 100 µg/ml hygromycin at 37°C for 5 days. At the end of culture, the medium was collected and centrifuged to remove precipitates. The supernatants were passed over a 1-ml column of Protein G agarose (Invitrogen, Carlsbad, CA, USA) equilibrated with PBS. The column was then washed with PBS and the bound protein was eluted with 0.1 M sodium phosphate buffer, pH 2.6. Fractions containing EC-Fc were readily neutralized with sodium phosphate buffer, pH 8.0 by adding 1/10 volume of each fraction. The buffer was then replaced with PBS using a PD-10 column (GE Healthcare, Piscataway, NJ). The preparation of Fc protein without EC-1 moiety was based on the same procedure.

Competition EIA to estimate K_d value

The value of dissociation constant (K_d) between the ligand and ErbB2 was estimated as previously described with slight modification [24, 28]. Briefly, each well of 96-well plate was coated with 200 ng of sErbB2 in 0.1 M sodium bicarbonate buffer, pH 8.6, overnight at 4°C followed by blocking with PBS containing 1% BSA. After the rinse with PBS containing 0.1% Tween 20 (PBST), EC-Fc and varying concentration of sErbB2, which were premixed 30 min before, was applied to the wells. After the incubation for 30 min at 25 °C, the wells were washed with PBST and 50 µl of protein A-HRP conjugate (Sigma-Aldrich) diluted to 1:10,000 was added and incubated for 1 hr. Wells were then washed eight times with PBST and 100 µl of OPD solution was added for the HRP reaction. After 15 min, the reaction was quenched by 50 µl of 0.5 M sulphuric acid and the absorbance at 492 nm of each well was measured by a microplate reader MTP-120 (Corona, Japan). Each experiment was performed in triplicate and the mean values and standard deviations were calculated.

Preparation of multivalently displayed EC-1 peptide on bionanocapsule

To prepare the multivalent form of EC-1 peptide, EC-Fc proteins were displayed on the surface of bionanocapsule (BNC), which was composed of the recombinant surface antigen of hepatitis B virus [29]. To confer the high affinity for IgG Fc domain to BNC, the surface antigen was designed to fuse with the ZZ motif in the protein A derived from *Staphylococcus aureus* [25]. The resultant ZZ-tagged BNC (ZZ-BNC) was labelled with FITC by incubating with 1 mg/ml of FITC at 25°C for 15 min and the reaction mixture was further incubated at 4°C overnight in 0.1 M sodium bicarbonate buffer, pH 8.6. The molar ratio of FITC to ZZ-BNC was 110 to 1. After incubation, free FITC was removed by PD-10 column equilibrated with PBS. To prepare multivalently displayed form of EC-1 peptide, the molar ratio of ligand and BNC was optimized using Fc protein and human IgG (Sigma-Aldrich). To optimize the ratio FITC-labelled ZZ-BNC was mixed and incubated with Fc protein or human IgG at different ratio of 1:10, 1:20, 1:40, 1:60, 1:80 and 1:100 for 1 hr at 4°C. The precipitates formed were removed by centrifugation at 13,000 rpm for 5 min and the supernatant was transferred to a 96-black-well plate and fluorescence intensity at 530 nm of each well was measured by a microplate reader MTP-800 (Corona, Japan). Each experiment was performed in triplicate and the mean values and standard deviations were calculated. To characterize binding capacity of EC-Fc protein to ZZ-BNC, EC-Fc protein and ZZ-BNC were mixed in different ratios and incubated for 1 hr at 4°C. After centrifugation, the EC-Fc/BNC complex in the supernatant was immunoprecipitated with